12. Sekido Y, Pass HI, Bader S, *et al*: Neurofibromatosis type 2 (NF2) gene is somatically mutated in mesothelioma but not in lung cancer. Cancer Res 55: 1227-1231, 1995.
13. Bianchi AB, Mitsunaga SI, Cheng JQ, *et al*: High frequency of inactivating mutations in the neurofibromatosis type 2 gene (NF2) in primary malignant mesotheliomas. Proc Natl Acad Sci USA 92: 10854-10858, 1995.
14. Sekido Y, Bader S, Latif F, *et al*: Human semaphorins A(V) and IV reside in the 3p21.3 small cell lung cancer deletion region and demonstrate distinct expression patterns. Proc Natl Acad Sci USA 93: 4120-4125, 1996.
15. Lerman MI and Minna JD: The 630-kb lung cancer homozygous deletion region on human chromosome 3p21.3: identification and evaluation of the resident candidate tumor suppressor genes. The International Lung Cancer Chromosome 3p21.3 Tumor Suppressor Gene Consortium. Cancer Res 60: 6116-6133, 2000.
16. Hesson LB, Cooper WN and Latif F: Evaluation of the 3p21.3 tumour-suppressor gene cluster. Oncogene 26: 7283-7301, 2007.
17. Murthy SS and Testa JR: Asbestos, chromosomal deletions, and tumor suppressor gene alterations in human malignant mesothelioma. J Cell Physiol 180: 150-157, 1999.
18. Strizzi L, Catalano A, Vianale G, *et al*: Vascular endothelial growth factor is an autocrine growth factor in human malignant mesothelioma. J Pathol 193: 468-475, 2001.
19. Hirayama N, Tabata C, Tabata R, *et al*: Pleural effusion VEGF levels as a prognostic factor of malignant pleural mesothelioma. Respir Med 105: 137-142, 2011.
20. Yasumitsu A, Tabata C, Tabata R, *et al*: Clinical significance of serum vascular endothelial growth factor in malignant pleural mesothelioma. J Thorac Oncol 5: 479-483, 2010.
21. Filho AL, Baltazar F, Bedrossian C, Michael C and Schmitt FC: Immunohistochemical expression and distribution of VEGFR-3 in malignant mesothelioma. Diagn Cytopathol 35: 786-791, 2007.
22. Bielenberg DR, Pettaway CA, Takashima S and Klagsbrun M: Neuropilins in neoplasms: expression, regulation, and function. Exp Cell Res 312: 584-593, 2006.
23. Soker S, Takashima S, Miao HQ, Neufeld G and Klagsbrun M: Neuropilin-1 is expressed by endothelial and tumor cells as an isoform-specific receptor for vascular endothelial growth factor. Cell 92: 735-745, 1998.
24. Miao HQ, Soker S, Feiner L, Alonso JL, Raper JA and Klagsbrun M: Neuropilin-1 mediates collapsin-1/semaphorin III inhibition of endothelial cell motility: functional competition of collapsin-1 and vascular endothelial growth factor-165. J Cell Biol 146: 233-242, 1999.
25. Gaur P, Bielenberg DR, Samuel S, *et al*: Role of class 3 semaphorins and their receptors in tumor growth and angiogenesis. Clin Cancer Res 15: 6763-6770, 2009.
26. Serini G, Maione F, Giraudo E and Bussolino F: Semaphorins and tumor angiogenesis. Angiogenesis 12: 187-193, 2009.
27. Tamagnone L, Artigiani S, Chen H, *et al*: Plexins are a large family of receptors for transmembrane, secreted, and GPI-anchored semaphorins in vertebrates. Cell 99: 71-80, 1999.
28. Neufeld G and Kessler O: The semaphorins: versatile regulators of tumour progression and tumour angiogenesis. Nat Rev Cancer 8: 632-645, 2008.
29. Guttmann-Raviv N, Shraga-Heled N, Varshavsky A, Guimaraes-Sternberg C, Kessler O and Neufeld G: Semaphorin-3A and semaphorin-3F work together to repel endothelial cells and to inhibit their survival by induction of apoptosis. J Biol Chem 282: 26294-26305, 2007.
30. Kigel B, Varshavsky A, Kessler O and Neufeld G: Successful inhibition of tumor development by specific class-3 semaphorins is associated with expression of appropriate semaphorin receptors by tumor cells. PLoS One 3: e3287, 2008.
31. Toyofuku T, Zhang H, Kumanogoh A, *et al*: Dual roles of Sema6D in cardiac morphogenesis through region-specific association of its receptor, plexin-A1, with offtrack and vascular endothelial growth factor receptor type 2. Genes Dev 18: 435-447, 2004.
32. Catalano A, Lazzarini R, Di Nuzzo S, Orciari S and Procopio A: The plexin-A1 receptor activates vascular endothelial growth factor-receptor 2 and nuclear factor-kappaB to mediate survival and anchorage-independent growth of malignant mesothelioma cells. Cancer Res 69: 1485-1493, 2009.
33. Sato A, Torii I, Tao LH, *et al*: Establishment of a cell line from Japanese patient useful to generate an in vivo model for malignant pleural mesothelioma. Cancer Sci 102: 648-655, 2011.
34. Nannya Y, Sanada M, Nakazaki K, *et al*: A robust algorithm for copy number detection using high-density oligonucleotide single nucleotide polymorphism genotyping arrays. Cancer Res 65: 6071-6079, 2005.
35. Andersen CL, Lamy P, Thorsen K, *et al*: Frequent genomic loss at chr16p13.2 is associated with poor prognosis in colorectal cancer. Int J Cancer (In press).
36. Ivanov SV, Miller J, Lucito R, *et al*: Genomic events associated with progression of pleural malignant mesothelioma. Int J Cancer 124: 589-599, 2009.
37. Luo Y, Raible D and Raper JA: Collapsin: a protein in brain that induces the collapse and paralysis of neuronal growth cones. Cell 75: 217-227, 1993.
38. Castro-Rivera E, Ran S, Brekken RA and Minna JD: Semaphorin 3B inhibits the phosphatidylinositol 3-kinase/Akt pathway through neuropilin-1 in lung and breast cancer cells. Cancer Res 68: 8295-8303, 2008.
39. Capparuccia L and Tamagnone L: Semaphorin signaling in cancer cells and in cells of the tumor microenvironment-two sides of a coin. J Cell Sci 122: 1723-1736, 2009.
40. Ferrara N: Vascular endothelial growth factor as a target for anticancer therapy. Oncologist 9 (Suppl 1): S2-S10, 2004.
41. Karayan-Tapon L, Wager M, Guilhot J, *et al*: Semaphorin, neuropilin and VEGF expression in glial tumours: SEMA3G, a prognostic marker? Br J Cancer 99: 1153-1160, 2008.
42. Ito M, Ito G, Kondo M, *et al*: Frequent inactivation of RASSF1A, BLU, and SEMA3B on 3p21.3 by promoter hypermethylation and allele loss in non-small cell lung cancer. Cancer Lett 225: 131-139, 2005.
43. Tischoff I, Markwarth A, Witzigmann H, *et al*: Allele loss and epigenetic inactivation of 3p21.3 in malignant liver tumors. Int J Cancer 115: 684-689, 2005.
44. Ivanova AV, Ivanov SV, Prudkin L, *et al*: Mechanisms of FUS1/TUSC2 deficiency in mesothelioma and its tumorigenic transcriptional effects. Mol Cancer 8: 91, 2009.
45. Catalano A, Caprari P, Rodilossi S, *et al*: Cross-talk between vascular endothelial growth factor and semaphorin-3A pathway in the regulation of normal and malignant mesothelial cell proliferation. FASEB J 18: 358-360, 2004.

Pharmacokinetics of gefitinib and erlotinib

In a Comment[1] on the OPTIMAL trial,[2] Tetsuya Mitsudomi suggests that differences in clinical activity between the oral kinase inhibitors erlotinib and gefitinib in *EGFR* mutation-positive non-small-cell lung cancer could be attributable to their respective areas under the serum concentration–time curve (AUC). Erlotinib has a seven-times greater AUC than does gefitinib, which might explain its better clinical activity.

However, the activities of two chemically different drugs cannot be compared based solely on their AUC (by contrast with the comparison between two chemically identical agents, such as a generic and reference drug). The AUC depicts variations of blood concentrations over time after administration of a specific drug, at a specific dose. Pharmacokinetic characteristics that might cause differences in the activities of two drugs usually relate to tissue diffusion (if the target is extravascular) and elimination. Gefitinib has a perhaps more favourable pharmacokinetic profile than does erlotinib, with a longer elimination half-life (50·5 h *vs* 16·5 h) and a larger tissue distribution.[3] Differences in clinical activities between erlotinib and gefitinib might instead be explained by differences in their enzymatic inhibitory potential in situ and their duration of action.

I declare that I have no conflicts of interest.

Dominique Levêque
dominique.leveque@chru-strasbourg.fr
Hôpitaux Universitaires de Strasbourg, Strasbourg, France

1 Mitsudomi T. Erlotinib, gefitinib, or chemotherapy for *EGFR* mutation-positive lung cancer? *Lancet Oncol* 2011; **12**: 710–11.
2 Zhou C, Wu Y-L, Chen G, et al. Erlotinib versus chemotherapy as first-line treatment for patients with advanced *EGFR* mutation-positive non-small-cell lung cancer (OPTIMAL, CTONG-0802): a multicentre, open-label, randomised, phase 3 study. *Lancet Oncol* 2011; **12**: 735–42.
3 Scholler J, Levêque D. Molecular pharmacokinetic determinants of anticancer kinase inhibitors in humans. *Oncol Rev* 2011; **5**: 77–92.

The MARS feasibility trial: conclusions not supported by data

The value of extrapleural pneumonectomy (EPP) in the context of multimodality therapy for patients with malignant pleural mesothelioma is controversial. Several phase 2 studies have been reported on the role of neoadjuvant chemotherapy, EPP, and postoperative radiotherapy. These studies have included patients with T1–3 tumours, but differed in the inclusion of N2 status and sarcomatoid histology. Around three-quarters of patients included in these trials underwent EPP and about three-fifths received post-operative radiotherapy. Median survival ranged from 16·8 to 25·5 months, and the operative mortality from EPP from 0% to 5% (table).[1–6]

Independent assessment of the distinct components of a multi-modality concept is desirable, especially of radical surgery and post-operative radiotherapy, because both have a more pronounced potential to affect survival than does chemo-therapy alone. The MARS trial[7] attempted to assess the efficacy of EPP, and an ongoing SAKK trial is assessing the value of postoperative radio-therapy after neoadjuvant chemo-therapy and EPP (ClinicalTrials.gov identifier NCT00334594).

Because of the anticipated difficulty in recruitment of patients to a trial comparing EPP with a non-surgical approach, the MARS researchers designed a feasibility trial with the objective of randomly assigning 50 patients within 1 year to assess the possibility of completing a larger trial to clarify the role of EPP. The study was therefore not designed to test the benefit (or absence thereof) of EPP for patient outcome, and any conclusions are speculative. Moreover, this feasibility study failed, because it took 3 years to accrue 50 patients.

According to the investigators of the MARS trial, 670 patients would be needed to identify any significant difference in overall survival between EPP and no EPP. However, the survival results reported in *The Lancet Oncology*[7] are based on only 30 deaths. Thus, no firm conclusion can be drawn about the effect of EPP on overall survival from these data.

	Stage	Number of patients			ITT median survival (95% CI)	EPP operative mortality
		Chemotherapy	EPP	Radiotherapy		
Weder and colleagues[1]	T1–3, N0–2	19 (100%)	16 (84%)	13 (68%)	23	0%
Weder and colleagues[2]	T1–3, N0–2	61 (100%)	45 (74%)	36 (59%)	19·8 (14·6–24·5)	2·2%
Rea and colleagues[3]	T1–3, N0–2	21 (100%)	17 (81%)	15 (71%)	25·5	0%
Batirel and colleagues[4]	T1–3, N0–2	20 (100%)	16 (80%)	12 (60%)	17	5%
Krug and colleagues[5]	T1–3, N0–2	77 (100%)	57 (74%)	44 (57%)	16·8 (13·6–23·2)	3·7%
Van Schil and colleagues[6]	T1–3, N0–2	59 (100%)	42 (73%)	38 (64%)	18·4 (15·6–32·9)	5%

ITT=intention to treat. Median survival is in months.

Table: Prospective studies of trimodality therapy of malignant pleural mesothelioma including neoadjuvant chemotherapy, extrapleural pneumonectomy (EPP), and radiotherapy

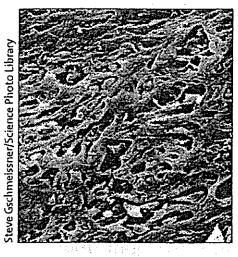
Steve Gschmeissner/Science Photo Library

112 patients were registered in this study and 50 (42%) were randomly assigned to treatment. Eligibility for randomisation was determined by CT restaging after chemotherapy and assessment by a multidisciplinary team. No information about the status of the 58% of patients not considered eligible for randomisation is provided in the report; however, these patients were presumably deemed to be unfit for surgery because of tumour progression or other compromising conditions. Therefore the reported survival results cannot be compared directly with results of the prospective multimodality studies in the table,[1-6] in which survival is reported by intention to treat from the start of any therapy.

In the MARS study[7] a few factors can be identified that could further affect the interpretation. First, the chemotherapy delivered in MARS before randomisation was not standardised for type and dose of drugs or for number of cycles, which generates difficulties in assessing such small numbers of events. Second, no data are provided about the time from beginning of chemotherapy to EPP. In a multidisciplinary treatment approach, the time allowed between the different treatments should be fixed and as short as possible. Lastly, it is important to know whether the surgical triage of 19 of 24 patients having an attempted EPP, of whom only 16 eventually completed EPP, was related to undue treatment delays. Moreover, three patients in the non-surgical group eventually did undergo EPP and three additional patients had non-EPP surgery. These protocol violations further complicate interpretation.

EPP is the focus of the MARS feasibility trial. However, within the context of MARS the operative mortality for the 17 patients who underwent EPP per protocol was 18%. By contrast, recently reported trials for trimodality therapy including EPP show mortality of 0–5%.[1-6] In view of the small number of patients in the MARS study, this high mortality could be a statistical anomaly, but nevertheless, is a concern.

The MARS study did not show the feasibility of doing a trial comparing chemotherapy with EPP and radiotherapy. We believe the interpretation of the study—"These data, although limited, suggest that radical surgery in the form of EPP within trimodal therapy offers no benefit and possibly harms patients"—is inappropriate, could move clinical research for mesothelioma in the wrong direction, and might be harmful to patients seeking advice.

We declare that we have no conflicts of interest.

*Walter Weder, Rolf A Stahel, Paul Baas, Urania Dafni, Marc de Perrot, Brian C McCaughan, Takashi Nakano, Harvey I Pass, Bruce W S Robinson, Valerie W Rusch, David J Sugarbaker, Nico van Zandwijk
walter.weder@usz.ch

Division of Thoracic Surgery (WW) and Clinic of Oncology (RAS), University Hospital Zurich, Zurich, Switzerland (WW); Academic Medical Center, The Netherlands Cancer Institute, Amsterdam, Netherlands (PB); Division Laboratory of Biostatistics, University of Athens, and Frontier Science Foundation-Hellas, Athens, Greece (UD); Division of Thoracic Surgery, University of Toronto, Toronto, ON, Canada (MdP); Department of Cardio-thoracic Surgery (MdP), The Baird Institute, Royal Prince Alfred Hospital, University of Sydney, Sydney, NSW, Australia (BCMcC); Division of Respiratory Medicine/ Department of Internal Medicine, Department of Thoracic Oncology, Hyogo College of Medicine, Nishinomiya, Hyogo, Japan (TN); Department of Cardiothoracic Surgery, Thoracic Surgery NYU Langone Medical Center New York, NY, USA (HIP); National Centre for Asbestos Related Diseases, School of Medicine and Pharmacology, Sir Charles Gairdner Hospital, Perth, WA, Australia (BWSR); Thoracic Surgery Service, Memorial Sloan-Kettering Cancer Center, New York, NY, USA (VWR); Division of Thoracic Surgery, Brigham and Women's Hospital, Harvard Medical School, Boston, MA, USA (DJS); and Asbestos Diseases Research Institute, University of Sydney Bernie Banton Centre, Concord, NSW, Australia (NvZ)

1 Weder W, Kestenholz P, Taverna C, et al. Neoadjuvant chemotherapy followed by extrapleural pneumonectomy in malignant pleural mesothelioma. *J Clin Oncol* 2004; **22**: 3451–57.
2 Weder W, Stahel R, Bernhard J, et al, for the Swiss Group for Clinical Cancer Research. Multicenter trial of neo-adjuvant chemotherapy followed by extrapleural pneumonectomy in malignant pleural mesothelioma. *Ann Oncol* 2007; **18**: 1196–202.
3 Rea F, Marulli G, Bortolotti L, et al. Induction chemotherapy, extrapleural pneumonectomy (EPP) and adjuvant hemi-thoracic radiation in malignant pleural mesothelioma (MPM): feasibility and results. *Lung Cancer* 2007; **57**: 89–95.
4 Batirel HF, Metintas M, Caglar HB, et al. Trimodality treatment of malignant pleural mesothelioma. *J Thorac Oncol* 2008; **3**: 499–504.
5 Krug LM, Pass HI, Rusch VW, et al. Multicenter phase II trial of neoadjuvant pemetrexed plus cisplatin followed by extrapleural pneumonectomy and radiation for malignant pleural mesothelioma. *J Clin Oncol* 2009; **27**: 3007–13.
6 Van Schil PE, Baas P, Gaafar R, et al, for the European Organisation for Research and Treatment of Cancer (EORTC) Lung Cancer Group. Trimodality therapy for malignant pleural mesothelioma: results from an EORTC phase II multicentre trial. *Eur Respir J* 2010; **36**: 1362–69.
7 Treasure T, Lang-Lazdunski L, Waller D, et al. Extra-pleural pneumonectomy versus no extra-pleural pneumonectomy for patients with malignant pleural mesothelioma: clinical outcomes of the Mesothelioma and Radical Surgery (MARS) randomised feasibility study. *Lancet Oncol* 2011; **12**: 763–72.

Authors' reply

Apart from MARS,[1] evidence relating to extra-pleural pneumonectomy (EPP) for mesothelioma comes from uncontrolled studies. Large follow-up studies report median survivals of 12, 13, and 14 months in 385, 121, and 208 patients, respectively. Small prospective studies report median survival in the range of 1–2 years, on intention to treat from the start of the planned trimodal treatment. The equivalent measure of survival in MARS was 18 months (14·4 months after randomisation plus 3·6 months from registration). These data and citations are provided in our Article along with full details and discussion about the significance of two patients in the EPP group who died within 30 days.[1]

What sets MARS apart is that after completion of chemotherapy, eligible patients were randomly allocated to EPP and radical

Cancer Science
The official journal of the Japanese Cancer Association JCA

Establishment of a cell line from a Japanese patient useful for generating an *in vivo* model of malignant pleural mesothelioma

Ayuko Sato,[1] Ikuko Torii,[1] Li-Hua Tao,[1] Misa Song,[1] Nobuyuki Kondo,[2] Yoshie Yoshikawa,[3] Tomoko Hashimoto-Tamaoki,[3] Seiki Hasegawa,[2] Takashi Nakano[4] and Tohru Tsujimura[1,5]

Departments of [1]Pathology, [2]General Thoracic Surgery, [3]Genetics, Hyogo College of Medicine, Hyogo; [4]Division of Respiratory Medicine, Department of Internal Medicine, Hyogo College of Medicine, Hyogo, Japan

(Received October 15, 2010/Revised November 29, 2010/Accepted December 2, 2010/Accepted manuscript online December 9, 2010/Article first published online January 18, 2011)

Malignant pleural mesothelioma is a refractory tumor with increasing incidence. In the present study, we established six mesothelioma cell lines possessing two allele deletions of the *p16^{INK4A}* gene and one allele deletion of the *neurofibromatosis type 2* gene, MM16, MM21, MM26, MM35, MM46 and MM56, from pleural effusion fluids or surgically resected tumors of Japanese patients. MM21, MM26 and MM46 cells failed to develop tumors in BALB/c-nude mice following subcutaneous inoculation. MM16 and MM35 cells slowly generated tumors at the site of subcutaneous inoculation in BALB/c-nude mice, but lost the expression of mesothelioma-related markers such as calretinin, D2-40 and Wilms' tumor 1 in the subcutaneous tumors. On the other hand, MM56 cells rapidly generated tumors with the expression of calretinin and D2-40 in BALB/c-nude mice following subcutaneous inoculation. In addition, orthotopic implantation of MM56 cells into BALB/c-nude mice developed diffusely growing thoracic tumors by 3 weeks after implantation. Pleural effusions were observed in these mice 4 weeks after implantation. Thoracic tumors invaded aggressively into the chest wall 5 weeks after implantation and often metastasized into the lung, rib, peritoneum and pericardial cavity. On the pleural surface, MM56 cells were growing as single or multiple cell layers with the reactive mesothelium of recipient mice. These results indicate that MM56 cells can behave in a manner characteristic of human malignant pleural mesothelioma in the thoracic cavity of BALB/c-nude mice. The *in vivo* model using MM56 cells may be useful for studying the biological behavior of malignant pleural mesothelioma and developing its diagnostic and therapeutic strategies. (*Cancer Sci* 2011; 102: 648–655)

Malignant pleural mesothelioma (MPM), considered to be closely associated with asbestos exposure, is an aggressive tumor arising from mesothelial cells on the serosal surfaces of the thoracic cavity. Malignant pleural mesothelioma was once a rare disease, but its incidence is dramatically increasing worldwide. In Japan, it is expected to peak around 2025 as a result of widespread use of asbestos.[1] Malignant pleural mesothelioma is often diagnosed at an advanced stage and known to be resistant to conventional therapies. As a result it is associated with poor prognosis, with the median survival in the range of 9–17 months after the first diagnosis.[2] It is therefore important to establish a means for investigating the behaviors of MPM, leading to the development of early diagnosis and effective therapies.

Cell lines and animal models of human tumors are useful for studying the characteristics of tumors. Several MPM cell lines have been established[3–5] and animal models have been produced by inoculation of MPM cells or surgically resected MPM tissues into immunodeficient mice or rats.[6–9] Orthotopic implantation models are considered to be the most useful for studying the characteristics of MPM *in vivo*,[10–12] but most require a long period to develop MPM after implantation and often they have not reproduced the biological features of MPM well. In the pathological diagnosis of MPM, the distinction between MPM and reactive mesothelium (RM) is challenging because of the similar morphology and lack of reliable discriminating markers.[13,14] This problem may be resolved by establishing an experimental system that allows analysis of the morphological and immunohistological differences of MPM and RM on the pleural surface.

In the present study, we established six cell lines of MPM and found that one of them, termed MM56, exhibited the ability to reproduce the characteristic features of human MPM in BALB/c-nude mice. The *in vivo* model using MM56 cells might be useful for studying the biological behaviors of MPM and developing its diagnostic and therapeutic approaches.

Materials and Methods

Establishment of MPM cell lines. Pleural effusion fluids and tumor tissues were obtained from Japanese patients diagnosed with MPM by histopathological examinations of pleural biopsy at the Hospital of Hyogo College of Medicine (Table 1). Cells in pleural effusion fluids were collected by centrifugation at 440*g* for 10 min and cultured in α-MEM (Invitrogen, Carlsbad, CA, USA) supplemented with 10% FBS (Equitech-Bio, Ingram, TX, USA), 100 U/mL penicillin (Sigma, St Louis, MO, USA) and 100 μg/mL streptomycin (Wako Pure Chemical Industries, Osaka, Japan). Adherent cells were cultured in a 37°C/5% CO_2 humidified incubator to establish the MPM cell lines. Surgically resected tumors were cut into small pieces after removal of adipose tissues. Tissue pieces were plated on culture dishes, gently overlaid with culture medium and maintained in a 37°C/5% CO_2 humidified incubator to establish the MPM cell lines.

This study was approved by the Ethics Committee of Hyogo College of Medicine and performed in accordance with the Declaration of Helsinki (1995) of the World Medical Association (as revised in Tokyo 2004). All patients provided written informed consent.

Cell proliferation assay. Cells were plated in six-well plates 24 h before the cell proliferation assay. Adherent cells were harvested daily by 0.25% trypsin-EDTA treatment and the number of viable cells was calculated by the trypan blue exclusion method. The doubling time was determined at the log phase of cell proliferation.

Transmission electron microscopy. Cells were harvested by 0.25% trypsin-EDTA treatment and fixed in 2.5% phosphate-buffered glutaraldehyde for 30 min and in 1% phosphate-buffered

[5]To whom correspondence should be addressed. E-mail: tohru@hyo-med.ac.jp

doi: 10.1111/j.1349-7006.2010.01827.x

Table 1. Clinical characteristics and immunocyto/histochemical findings

Case/cell line	MM16	MM21	MM26	MM35	MM46	MM56
Sex	M	M	F	M	M	M
Age (years)	65	45	67	67	69	43
Asbestos exposure	+	+	+	+	+	+
Histological type	B	E	E	E	S	E
Source for culture	Tumor	Effusion	Tumor	Effusion	Effusion	Tumor
Immunocyto/histochemical findings						
Calretinin	+	+	+	+	−	+
D2-40	+	ND	+	+	−	+
WT-1	−	ND	+	ND	ND	ND
CK5/6	+	+	+	+	−	ND
CK (CAM5.2)	+	ND	ND	ND	ND	ND
CK (AE1/AE3)	+	ND	ND	ND	ND	+
CEA	−	−	−	−	−	−
TTF-1	−	−	−	−	−	−

Pleural effusion fluids and tumor tissues were obtained from Japanese patients diagnosed with MPM by histopathological examinations of pleural biopsy. Immunocyto/histochemical findings of pleural effusions or tumor tissues, which are used as the sources for the establishment of cultured cell lines, are shown. B, biphasic type; CEA, carcinoembryonic antigen; CK, cytokeratin; E, epithelioid type; F, female; M, male; MPM, malignant pleural mesothelioma; ND, not determined; S, sarcomatoid type; TTF-1, thyroid transcription factor 1; WT-1, Wilms' tumor 1.

OsO_4 for 15 min at room temperature. After dehydration, cells were embedded in epoxy resin and cut into 70-nm thickness. The sections were counterstained with uranil acetate and lead citrate and analyzed with a JEM-1220 electron microscope (JEOL, Tokyo, Japan).

Copy number analysis by real-time PCR. The copy number of the $p16^{INK4A}$ and the *neurofibromatosis type 2* (*NF2*) genes in the genomic DNA of MPM cells was analyzed by real-time PCR based on the dual-labeled fluorescent probe system, and determined by the comparative threshold cycle method using the *RPS6* gene as a control and the genomic DNA of human pleural mesothelial cells, MeT-5A, as a reference. The following sets of forward primer, reverse primer and probe designed by FastPCR were used for real-time PCR: 5′-cgggcgactctggaggacgaagtt, 5′-agatctgtacgcgcgtggctcctc and 5′FAM-ctgggggcttgggaagcca-Eclipse for the $p16^{INK4A}$ gene; 5′-acctctttgatttggtgtgccgga, 5′-gtccattttgagccaggccactg and 5′FAM-cacaatcaaggacacagtgg-cct-Eclipse for the *NF2* gene; and 5′-ggtttccccatgaagcagggtgtc, 5′-gagaacgctcagatttgcatccac and 5′FAM-tcagttcgtggttgcattgtgga-Eclipse for the *RPS6* gene. In the comparative threshold cycle method, the calculated value of 1.0 indicated no deletion, that of 0.5 indicated a one allele deletion and that of 0 indicated a two allele deletion.

Implantation of MPM cells into mice. Seven-week-old female BALB/c-nude mice were purchased from Japan SLC (Hamamatsu, Shizuoka, Japan) and maintained under specific pathogen-free conditions. The MPM cells (5×10^6 cells in 100 μL PBS) were injected subcutaneously into both flanks of BALB/c-nude mice, and the development of subcutaneous tumors was examined once a week. When tumors reached 1–2 cm in size, the mice were killed and the tumors were removed for histological examination. The tumor volume was calculated according to the formula: $V\ (mm^3) = ½ \times A \times B^2$, where A is the major axis and B is the minor axis.

For the orthotopic implantation model, MPM cells (3×10^6 cells in 100 μL PBS) were injected into the right thoracic cavity of BALB/c-nude mice through the intercostal space using a 29G needle after skin incision, as previously described.[10] After injection of the MPM cells, the incised skin was closed by 9 mm AUTOCLIP wound clips (Becton Dickinson, Sparks, MD, USA). The mice were killed and examined macroscopically for the development of tumors in the thoracic cavity on the scheduled day after inoculation or when they became moribund, whichever came first. The thoraces were removed from the mice for histological examination.

All experimental procedures were approved by the Animal Care Committee of Hyogo College of Medicine and performed in accordance with the criteria outlined in "Guide for the Care and Use of Laboratory Animals" prepared by the National Academy of Sciences (unpublished material).

Histocytological examinations. Cultured cells were harvested by trypsin-EDTA treatment, collected by centrifugation, fixed in 10% formalin neutral buffer solution, embedded in paraffin and cut into 3-μm-thick sections to generate cell block specimens. Tissues removed from the mice were fixed in 10% formalin neutral buffer solution, embedded in paraffin and cut into 3-μm thickness. For the whole thoraces, decalcification was performed with EDTA before embedding in paraffin. Cells in pleural effusion fluids developed in mice orthotopically implanted with MPM cells were collected by centrifugation and subjected to preparation of cell block specimens or smear specimens. Paraffin-embedded specimens were stained with HE and smear specimens were stained with Papanicolaou.

Immunohistochemistry. Specimens were heated to 98°C in Target Retrieval Solution (S1700; DakoCytomation, Glostrup, Denmark) or Target Retrieval Solution pH 9 (S2368; DakoCytomation), or incubated at room temperature with proteinase K (S3020; DakoCytomation) to facilitate antigen retrieval. Specimens of human origin were incubated with various mouse primary antibodies (Table 2) and sequentially with an anti-mouse immunoglobulin antibody using a ChemMate EnVision kit (DakoCytomation). Immunostaining with a rabbit anti-CD146 antibody (Table 2) was sequentially incubated with an anti-rabbit immunoglobulin using a ChemMate EnVision kit. For immunostaining of the mouse tissues with mouse primary antibodies, CAM5.2, calretinin and D2-40, a Histofine MOUSESTAIN kit (Nichirei Bioscience, Tokyo, Japan) was used to eliminate the background staining of endogenous mouse immunoglobulin. Immunoreacted cells were visualized with 3, 3′-diaminobenzidine, and the nuclei were lightly counterstained with hematoxylin.

Results

Establishment of MPM cell lines. Six cell lines, designated MM16, MM21, MM26, MM35, MM46 and MM56, were established from the pleural effusion fluids or surgically resected tumors of untreated Japanese patients with MPM (Table 1). These cells grew as an adherent monolayer (Fig. 1a) with the doubling time of 12.4 ± 0.9 h for MM16, 13.9 ± 0.4 h for MM21, 15.7 ± 1.3 h for MM26, 32.8 ± 2.5 h for MM35,

Table 2. Antibodies used in the present study

Antibody	Clone	Source	Dilution	Retrieval
Calretinin	DAK-Calret1	DakoCytomation	1:100	TRS, 20 min
D2-40	D2-40	DakoCytomation	1:50	TRS (pH 9), 20 min
WT-1	6F-H2	DakoCytomation	1:25	TRS, 40 min; ProK, 5 min
CK 5/6	D5/16 B4	DakoCytomation	1:50	TRS (pH 9), 40 min
CK (CAM5.2)	CAM5.2	Becton Dickinson	Pre-diluted	ProK, 5 min
CK (AE1/AE3)	AE1/AE3	DakoCytomation	1:100	TRS (pH 9), 20 min
CEA	II-7	DakoCytomation	1:50	TRS, 20 min
TTF-1	8G7G3/1	DakoCytomation	1:50	TRS (pH 9), 40 min
EMA	E29	DakoCytomation	1:40	None
CD146	EPR3208	Epitomics	1:200	TRS, 20 min

CD146 is a rabbit monoclonal antibody. Other antibodies used in the present study are mouse monoclonal antibodies. Source information with the manufacturers' location is as follows: DakoCytomation, Glostrup, Denmark; Becton Dickinson, San Jose, CA, USA; and Epitomics, Burlingame, CA, USA. CEA, carcinoembryonic antigen; CK, cytokeratin; EMA, epithelial membrane antigen; ProK, proteinase K; TRS, Target Retrieval Solution; TTF-1, thyroid transcription factor 1; WT-1, Wilms' tumor 1.

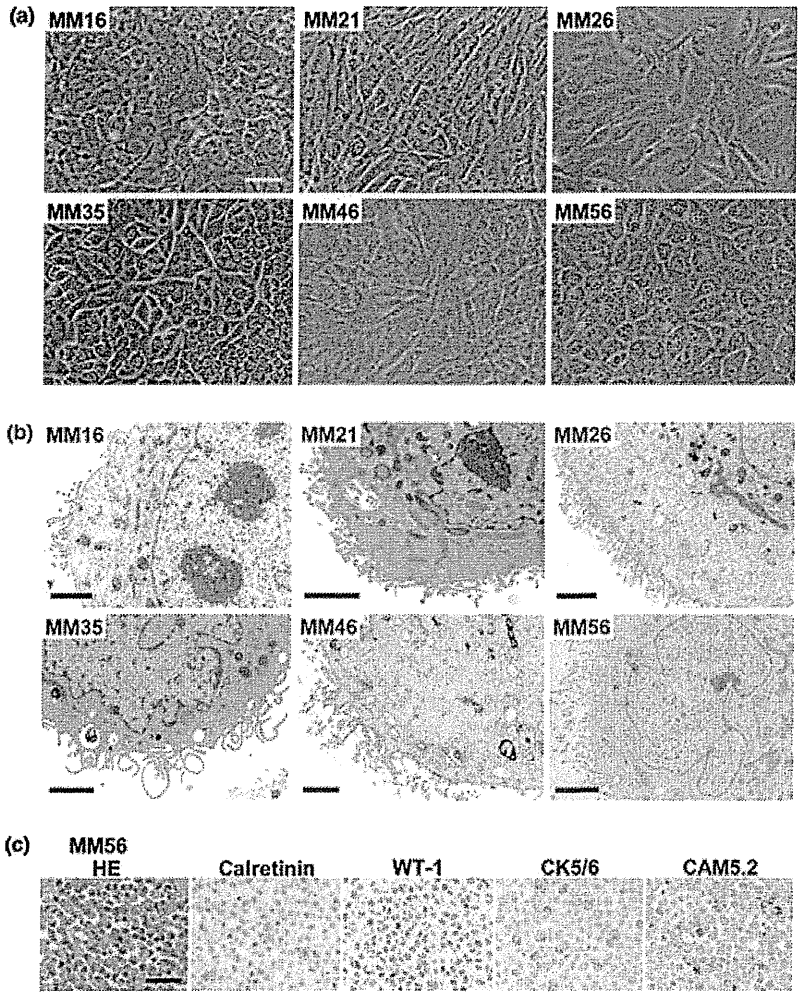

Fig. 1. Malignant pleural mesothelioma (MPM) cell lines, MM16, MM21, MM26, MM35, MM46 and MM56. (a) Phase-contrast microscopic analysis of cultured MPM cell lines. Scale bar, 50 μm. (b) Transmission electron microscopic analysis of cultured MPM cell lines. Scale bars, 2 μm. (c) HE staining of a cell block specimen and immunostaining of MM56 cells with antibodies to calretinin, Wilms' tumor 1 (WT-1), cytokeratin (CK) 5/6 and CK (CAM5.2). Scale bar, 50 μm.

11.5 ± 0.5 h for MM46 and 15.6 ± 1.8 h for MM56. Ultrastructural analysis revealed that these cells possessed numerous long, thin and irregular microvilli, which is characteristic of MPM, on the cell surface (Fig. 1b).

Immunostaining of the cell block specimens showed that all MM16, MM21, MM26, MM35, MM46 and MM56 cells were negative for carcinoma-related markers, carcinoembryonic antigen and thyroid transcription factor 1, but positive for both mesothelioma- and carcinoma-related markers, cytokeratin (CK) (clone CAM5.2) and CK (clone AE1/AE3). In addition, MM16, MM21, MM35 and MM56 cells were positive for mesothelioma-related markers, calretinin, D2-40, Wilms' tumor 1 (WT-1)

doi: 10.1111/j.1349-7006.2010.01827.x

and CK5/6, MM26 cells for calretinin, D2-40 and WT-1, and MM46 cells for WT-1 (Table 3, Fig. 1c). These results indicate that all established cell lines originated from MPM and that MM16, MM21, MM35 and MM56 cells maintained the immunohistological phenotype of MPM well.

To analyze the copy number of the $p16^{INK4A}$ and the *NF2* genes in the established cell lines, real-time PCR with the comparative threshold cycle method was performed. The value of the $p16^{INK4A}$ and the *NF2* genes was calculated as 0.01 and 0.53 for MM16, 0.02 and 0.39 for MM21, 0.01 and 0.53 for MM26, 0.01 and 0.52 for MM35, 0.00 and 0.22 for MM46, and 0.00 and 0.35 for MM56, respectively. These results indicated that two alleles of the $p16^{INK4A}$ gene and one allele of the *NF2* gene were deleted in all established cell lines.

Tumorigenicity of the MPM cell lines in BALB/c-nude mice. To examine the tumorigenic potential of the established cell lines, the MPM cells were injected subcutaneously into both flanks of the BALB/c-nude mice. The MM21, MM26 and MM46 cells failed to develop tumors at the site of inoculation. In contrast, the MM16 and MM56 cells formed tumors in all 12 mice (24 sites of both flanks) and the MM35 cells in nine of 12 mice (18 of 24 sites of flanks). The rate of tumor growth was examined in eight sites of four mice inoculated with MM16 and MM56 cells and in six sites of three mice inoculated with MM35 cells. MM56 tumors grew very aggressively, MM16 tumors grew moderately and MM35 tumors grew extremely slowly (Fig. 2a). The MM56 tumors were soft and rich in fluids, while MM16 and MM35 tumors were solid and firm. Immunostaining with anti-CAM5.2 antibody, which reacts to only human but not mouse CK, confirmed that MM16, MM35 and MM56 tumors arose from inoculated human MPM cells (Fig. 2b). The MM56 tumors retained immunoreactivity to mesothelioma-related markers, calretinin and D2-40 (Fig. 2c), whereas the MM16 and MM35 tumors lost immunoreactivity to these markers.

Orthotopic implantation model of MPM cell lines in BALB/c-nude mice. To generate an orthotopic implantation model of MPM cell lines, the MPM cells were inoculated orthotopically into the thoracic cavity of BALB/c-nude mice. As in subcutaneous implantation, MM21, MM26 and MM46 cells failed to develop thoracic tumors, but MM16, MM35 and MM56 cells were able to develop thoracic tumors. Orthotopic implantation of MM16 cells generated tumor nodules, but not diffusely growing tumors along the pleura, in the thoracic cavity 6 weeks after implantation. MM16 thoracic tumors lost expression of the mesothelioma-related markers (data not shown). Orthotopic implantation of the MM35 cells did not generate thoracic tumors in mice within 6 weeks after implantation. Some mice orthotopically inoculated with MM35 cells became moribund with pleural effusions and tumors in the thoracic cavities around 30 weeks after implantation (Fig. 3a,b). Cells in the pleural effusions of these mice grew in a papillary pattern and were CAM5.2 positive (Fig. 3c,d). Orthotopic implantation of MM56 cells generated thoracic tumors diffusely growing along the pleura and pleural effusions by 6 weeks after implantation (Fig. 3e,f). Cells in the pleural effusions showed MPM features with mirror ball-like cell clusters and multinucleated cells (Fig. 3g), and were CAM5.2 positive (data not shown). Histologically, CAM5.2-positive MM56 cells proliferated in the thoracic cavity (Fig. 3h,i) and grew along the parietal pleura of

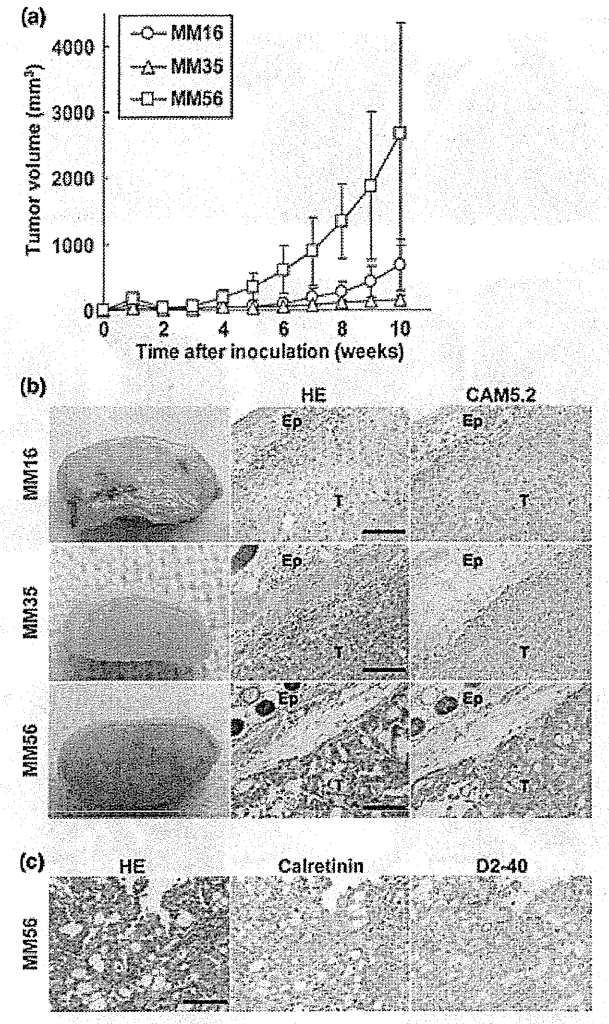

Fig. 2. Tumors developed from subcutaneously implanted MM16, MM35 and MM56 cells. (a) Growth of subcutaneous tumors. Each point represents the mean volume ± SEM of 6–8 tumors. (b) Macroscopic analysis and histological examination of subcutaneous tumors. The volume of MM16, MM35 and MM56 tumors was 3757 (after 9 weeks), 320 (17 weeks) and 3035 mm^3 (7 weeks), respectively. MM16, MM35 and MM56 tumors were stained with HE and immunostained with anti-CAM5.2 antibody. Scale bars, 100 μm. Ep, epithelium; T, subcutaneous tumor. (c) Immunoreactivity of MM56 subcutaneous tumor to mesothelioma-related markers. A MM56 subcutaneous tumor was stained with HE and immunostained with antibodies to calretinin and D2-40. Scale bar, 100 μm.

Table 3. Immunostaining of MPM cell lines using cell block specimens

Cell lines	MM16	MM21	MM26	MM35	MM46	MM56
Mesothelioma-related markers						
Calretinin	1+	2+	1+	2+	–	1+
D2-40	±	3+	3+	2+	–	1+
WT-1	2+	3+	1+	3+	2+	3+
CK5/6	2+	2+	–	3+	–	2+
Both mesothelioma- and carcinoma-related markers						
CK (CAM5.2)	3+	2+	2+	2+	1+	2+
CK (AE1/AE3)	3+	3+	3+	3+	3+	3+
Carcinoma-related markers						
CEA	–	–	–	–	–	–
TTF-1	–	–	–	–	–	–

Staining intensity was scored as follows: –, negative; ±, focal and very weak positive; 1+, weak positive; 2+, moderate positive; 3+, strong positive. CEA, carcinoembryonic antigen; CK, cytokeratin; MPM, malignant pleural mesothelioma; TTF-1, thyroid transcription factor 1; WT-1, Wilms' tumor 1.

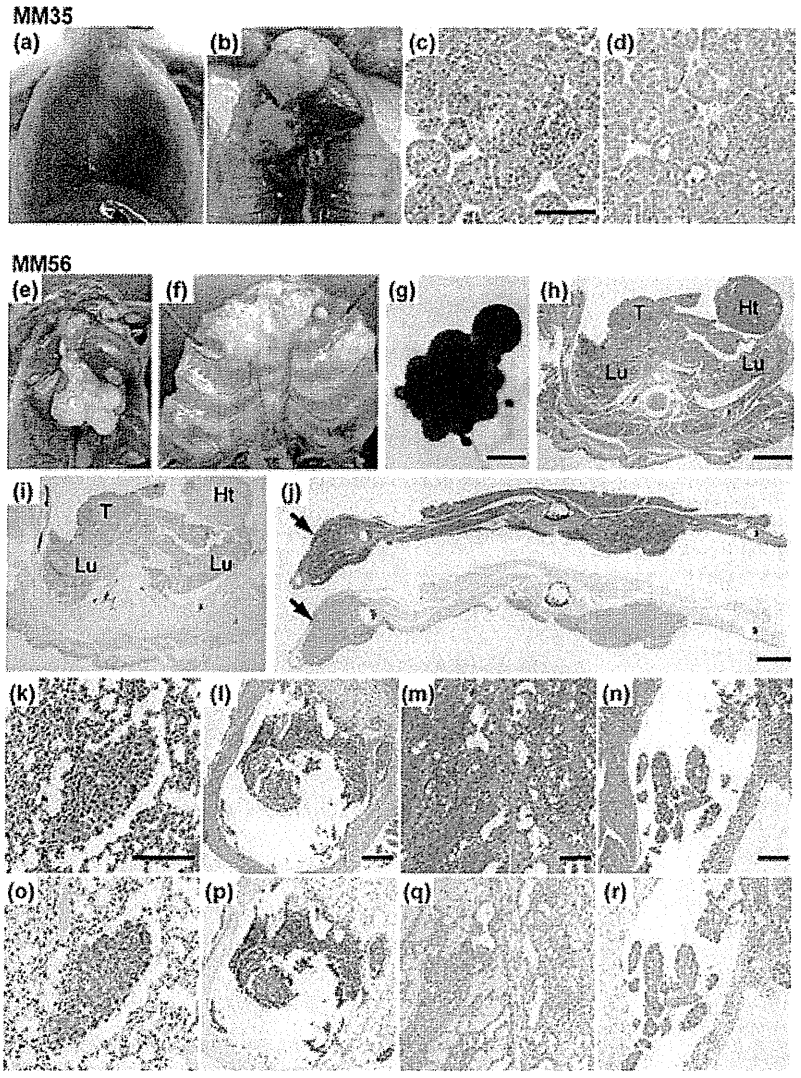

Fig. 3. Orthotopic implantation model of MM35 and MM56 cells. (a–d) A BALB/c-nude mouse 33 weeks after orthotopic inoculation with MM35 cells. (a) Pleural effusion fluids (700 μL) and MM35 thoracic tumors as observed from the abdominal cavity through the diaphragm. (b) MM35 thoracic tumors. (c) HE staining of a cell block specimen of pleural effusion. Scale bar, 100 μm. (d) Immunostaining of a cell block specimen of pleural effusion with anti-CAM5.2 antibody. (e–r) A BALB/c-nude mouse 6 weeks after orthotopic inoculation with MM56 cells. (e) MM56 thoracic tumors. (f) Diffuse growth involving the costal pleura of MM56 thoracic tumors. (g) Papanicolaou staining of a smear specimen of pleural effusion fluids (200 μL). Scale bar, 20 μm. (h) HE staining of the thorax. Scale bar, 2 mm. Ht, heart; Lu, lung; T, tumor. (i) Immunostaining of an adjacent specimen of (h) with anti-CAM5.2 antibody. (j) HE staining and immunostaining of the anterior chest wall shown in (f) with anti-CAM5.2 antibody. Arrows indicate tumor invasion at the inoculation site of the MM56 cells. Scale bar, 1 mm. (k–n) HE staining. Scale bars, 100 μm. (o–r) Immunostaining of an adjacent specimen of (k–n) with anti-CAM5.2 antibody. (k,o) Lung 3 weeks after implantation, (l,p) rib 5 weeks after implantation, (m,q) peritoneum 6 weeks after implantation, and (n,r) the pericardial cavity 7 weeks after implantation.

the anterior chest wall with invasion at the site of cell inoculation (Fig. 3j). Metastasis of MM56 thoracic tumors was often observed in the lung, rib, peritoneum and pericardial cavity throughout the experimental period (3–7 weeks) (Fig. 3k–r).

Utility of the MM56 orthotopic implantation model. Orthotopic implantation of MM56 cells resulted in the generation of thoracic tumors 3 weeks after implantation and pleural effusions 4 weeks after implantation (Table 4). Mice often became moribund around 7 weeks after implantation. Histologically, CAM5.2-positive cell clusters were observed in the thoracic cavity and CAM5.2-positive single or multiple cell layers spread along the pleural surface 3 weeks after implantation (Fig. 4a,b). Aggressive invasion of CAM5.2-positive cells into the chest wall was observed 5 weeks after implantation (Fig. 4c,d). These results indicate that MM56 cells grow in mice in a manner characteristic of human MPM.

To evaluate the utility of the MM56 orthotopic implantation model, thoracic tissues with MM56 cells were immunostained with anti-CD146 antibody that reacts to both human and mouse CD146, a marker discriminating between MPM (CD146-positive) and RM (CD146-negative).[15] As shown in Figure 4e–h, CAM5.2-positive MM56 cells growing in clusters in the thoracic cavity (black arrow heads) were positive for CD146.

Table 4. Tumorigenicity of the MM56 orthotopic implantation model

Weeks after inoculation	Incidence	
	Thoracic tumor	Pleural effusion
3	4/4	0/4
4	4/4	3/4
5	5/5	3/5
6	5/5	5/5
7	2/2	1/2

MM56 cells (3×10^6 cells in 100 μL PBS) were inoculated orthotopically into the right thoracic cavity of BALB/c-nude mice. The incidence of thoracic tumors and pleural effusions in recipient mice was examined at the indicated times.

CAM5.2-positive MM56 single or multiple cell layers along the pleural surface (black arrows) were also positive for CD146, whereas CAM5.2-negative mouse single cell layers on the pleural surface (white arrows) were negative. These results indicate that the coexistence of MPM and RM on the pleural surface is reproduced in the MM56 orthotopic implantation model.

doi: 10.1111/j.1349-7006.2010.01827.x

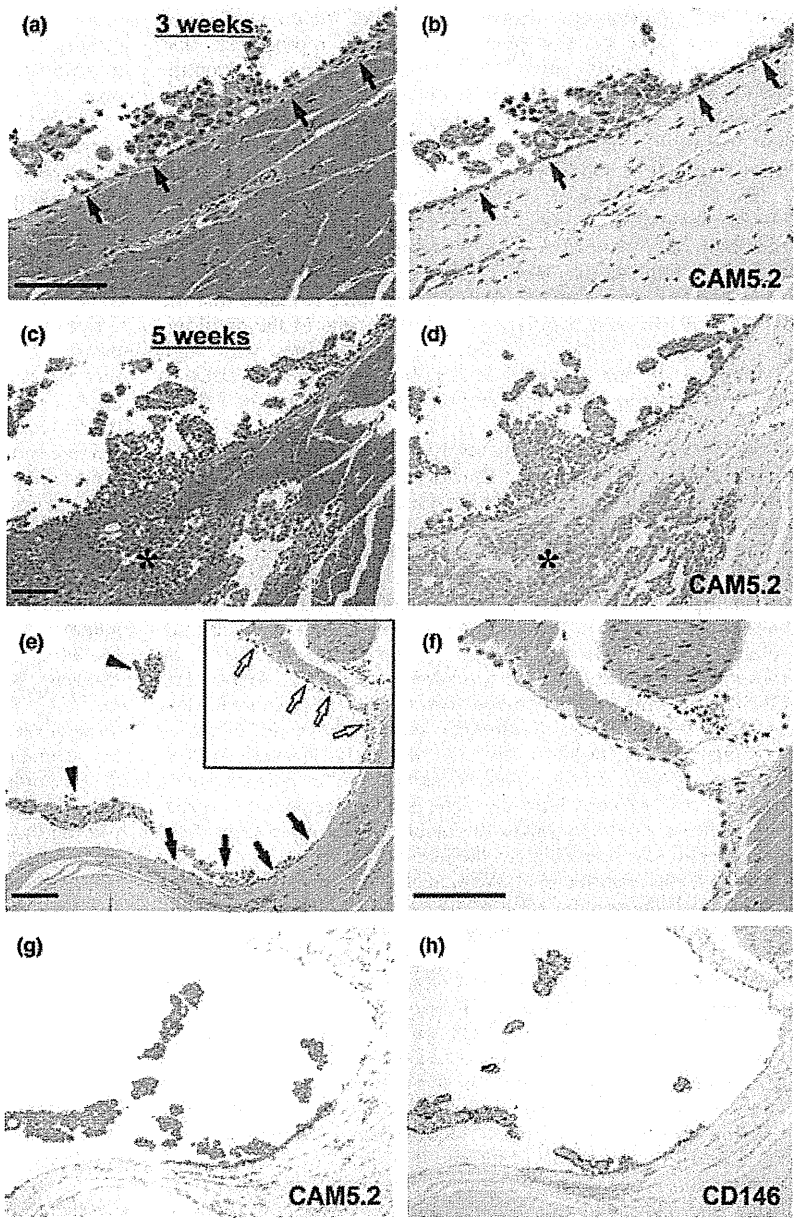

Fig. 4. Utility of MM56 orthotopic implantation model. (a–d) Progression of MM56 cells in the thoracic cavity. (a,b) A BALB/c-nude mouse 3 weeks after orthotopic inoculation with MM56 cells. (c,d) A BALB/c-nude mouse 5 weeks after orthotopic inoculation with MM56 cells. (a,c) HE staining of the thoracic cavity. (b,d) Immunostaining of adjacent specimens of (a,c) with anti-CAM5.2 antibodies. CAM5.2-positive MM56 cells proliferate in the thoracic cavity and diffusely grow along the pleural surface (black arrows) 3 weeks after MM56 inoculation (a, b). In a mouse 5 weeks after MM56 inoculation, CAM5.2-positive MM56 cells invade aggressively into the musculature of the chest wall (asterisks) (c,d). Scale bars, 100 μm. (e–h) Discrimination between malignant pleural mesothelioma (MPM) and reactive mesothelium (RM) in a MM56 orthotopic implantation model 6 weeks after inoculation. (e) HE staining of the thoracic cavity. (f) High magnification of the boxed area in (e). (g) Immunostaining of an adjacent specimen of (e) with anti-CAM5.2 antibody. (h) Immunostaining of an adjacent specimen of (e) with anti-CD146 antibody. Scale bars, 100 μm. Black arrow heads (cell clusters) and black arrows (single or multiple cell layers) indicate growing CAM5.2- and CD146-positive MM56 cells. White arrows (a single cell layer) indicate CAM5.2- and CD146-negative RM of a recipient mouse.

Discussion

In the present study we have established six mesothelioma cell lines, MM16, MM21, MM26, MM35, MM46 and MM56, from pleural effusion fluids or surgically resected tumors of untreated Japanese patients with MPM. The MM56 cell line was derived from a soft tumor of MPM consisting of polygonal cells partially with tubulopapillary or microcystic structures and expressing calretinin and D2-40. In addition, pleural effusion cytology of this MPM showed a cellular arrangement of sheets or mirror ball-like cell clusters. The MM56 cells formed subcutaneous tumors soft and rich in fluids and positive for calretinin and D2-40 in BALB/c-nude mice, indicating that the MM56 cells retain characteristic features of human MPM in BALB/c-nude mice. In addition, MM56 cells diffusely grew on the surface of parietal pleura with pleural effusions containing mirror ball-like cell clusters, invaded into the musculature of the chest wall and often metastasized into the lung, rib, peritoneum and pericardial cavity during 3–7 weeks after orthotopic implantation. Because MM56 cells could reproduce various stages of MPM from the earliest phases *in situ* to the advanced phases with metastasis within a short period in the BALB/c-nude mice, the MM56 orthotopic implantation model can be regarded as an excellent animal model for studying the biological behavior of human MPM *in vivo* and developing its diagnostic and therapeutic strategies.

Proliferation of atypical mesothelial cells on the pleural surface is considered as mesothelioma *in situ*, but it could only be diagnosed when accompanied by adjacent or subsequent invasive MPM.[16–19] Discrimination between early stage MPM and RM has been problematic due to morphological similarities and the lack of reliable discriminating markers.[13,14] On the other hand, we have recently reported that CD146 is a useful marker to discriminate MPM from RM in pleural effusion cytology.[15]

In the MM56 orthotopic implantation model, the coexistence of MPM and RM on the pleural surface is reproduced, and immunostaining with anti-CD146 antibody is able to identify MM56-derived MPM cells. Therefore, the MM56 orthotopic implantation model should be useful in detecting *in situ* lesions and identifying additional markers that discriminate between early stage MPM and RM.

The MM35 cells were less useful, because they slowly produced subcutaneous tumors in BALB/c-nude mice and thoracic tumors in only two of five mice 30 weeks after inoculation in an orthotopic implantation model. However, cytological analysis of the pleural effusion fluids in the recipient mice revealed that the MM35 cells formed papillary cell clusters, one of the cytological features of MPM.[20,21] Isolation of sublines with high tumorigenicity and MPM characteristics from pleural effusion fluids of recipient mice may improve the usefulness of MM35 cells.

Most human MPM grow diffusely in the thoracic cavity and a few proliferate as a nodule. The former is classified as diffuse MPM and the latter is classified as localized MPM. In addition, some MPM develop as multiple nodules in the thoracic cavity. Biopsy tissues of MPM, from which the MM16 cell line was established, were histologically biphasic mesothelioma growing as multiple nodules, but MPM at autopsy was sarcomatoid mesothelioma with a loss of expression of the mesothelioma-related markers. The MM16 cell line kept the expression of the mesothelioma-related markers, calretinin, D2-40, WT-1 and CK5/6, but MM16 subcutaneous and thoracic tumors were negative for these markers. Orthotopic inoculation of MM16 cells generated tumor nodules, but not diffusely growing tumors along the pleura, in the thoracic cavity of the BALB/c-nude mice. The MM16 subcutaneous and thoracic implantation models might be useful to clarify the mechanism(s) by which MPM grows as nodules and changes the phenotype.

It has been reported that WT-1, CAM5.2 and AE1/AE3 are expressed in more than 80% of sarcomatoid mesothelioma and the combined use of these markers provides the highest sensitivity in the differentiation of sarcomatoid mesothelioma from true sarcoma.[22] Consistent with this report, the MM46 cell line established from the sarcomatoid mesothelioma was positive for WT-1, CAM5.2 and AE1/AE3. Although sarcomatoid mesothelioma is highly malignant in human MPM, the MM46 cells failed to develop tumors in the BALB/c-nude mice. Previously, Usami *et al.*[4] established an epithelioid mesothelioma cell line, Y-MESO-8A, and a sarcomatoid mesothelioma cell line, Y-MESO-8D, from a biphasic mesothelioma consisting of epithelioid and sarcomatoid components, and reported that Y-MESO-8A cells, but not Y-MESO-8D cells, had the potential for developing a subcutaneous tumor in BALB/c-nude mice. Therefore, in sarcomatoid mesothelioma, it is unlikely that a correlation is observed between malignancy in human and tumorigenicity in nude mice. The MM46 cells may be useful to study the characteristic features of sarcomatoid mesothelioma.

The $p16^{INK4A}$ gene is the most frequently inactivated tumor suppressor gene in human MPM, and ~90% of MPM possesses deletions of the $p16^{INK4A}$ gene.[23] Abnormalities of the $p16^{INK4A}$ gene take part in the dysregulation of the cell cycle leading to malignant transformation of mesothelial cells. The *NF2* tumor suppressor gene is also frequently mutated in MPM. Recently, Yokoyama *et al.*[24] reported that mutation of the *NF2* gene promotes MPM proliferation through activation of YAP1, a transcriptional coactivator functionally inhibited by Merlin, a product of the *NF2* gene. In all six cell lines established in the present study, two allele deletions of the $p16^{INK4A}$ gene and one allele deletion of the *NF2* gene were found, which supports the theory that abnormalities of the $p16^{INK4A}$ and the *NF2* genes participate in the development of MPM. On the other hand, there is a possibility that abnormalities other than the $p16^{INK4A}$ and the *NF2* genes are related to the difference of tumorigenicity in nude mice among these six cell lines.

Novel biological therapies for MPM are under investigation.[2] Effects of various inhibitors against angiogenic factor, tyrosine kinase, ribonuclease, histone deacetylase and proteasome on MPM patients have been studied without much success. Mesothelin and CD26, mesothelioma-associated cell surface antigens, have been reported to be an immunotherapeutic target.[25–27] Recently, CD146 has been identified as the surface antigen recognized by an internalizing single chain antibody that can deliver liposome-encapsulated small molecule drugs into the cytoplasm of mesothelioma cells.[28] Our earlier study showed that CD146 was expressed in MPM but not RM,[15] supporting the theory that CD146 can be used as an effective immunotherapeutic target of MPM. The MM56 subcutaneous and orthotopic implantation models may serve as suitable *in vivo* systems to evaluate this possibility and develop preclinical strategies.

Acknowledgments

This work was supported in part by Grants-in-Aid for Scientific Research and a Hitec Research Center Grant from the Ministry of Education, Science, Sports, Culture, and Technology of Japan, and Grants-in-Aid for Researchers, Hyogo College of Medicine. The authors thank Ms. Michiko Kakihana and Ms. Mio Ohkabe for their technical and secretarial assistance.

Disclosure Statement

The authors have no conflict of interest.

References

1 Robinson BW, Lake RA. Advances in malignant mesothelioma. *N Engl J Med* 2005; **353**: 1591–603.
2 Tsao AS, Wistuba I, Roth JA, Kindler HL. Malignant pleural mesothelioma. *J Clin Oncol* 2009; **27**: 2081–90.
3 Philippeaux MM, Pache JC, Dahoun S *et al.* Establishment of permanent cell lines purified from human mesothelioma: morphological aspects, new marker expression and karyotypic analysis. *Histochem Cell Biol* 2004; **122**: 249–60.
4 Usami N, Fukui T, Kondo M *et al.* Establishment and characterization of four malignant pleural mesothelioma cell lines from Japanese patients. *Cancer Sci* 2006; **97**: 387–94.
5 Kobayashi M, Takeuchi T, Ohtsuki Y. Establishment of three novel human malignant pleural mesothelioma cell lines: morphological and cytogenetical studies and EGFR mutation status. *Anticancer Res* 2008; **28**: 197–208.
6 Chahinian AP, Beranek JT, Suzuki Y *et al.* Transplantation of human malignant mesothelioma into nude mice. *Cancer Res* 1980; **40**: 181–5.
7 Colt HG, Astoul P, Wang X, Yi ES, Boutin C, Hoffman RM. Clinical course of human epithelial-type malignant pleural mesothelioma replicated in an orthotopic-transplant nude mouse model. *Anticancer Res* 1996; **16**: 633–9.
8 Le Pimpec-Barthes F, Bernard I, Abd Alsamad I *et al.* Pleuro-pulmonary tumours detected by clinical and chest X-ray analyses in rats transplanted with mesothelioma cells. *Br J Cancer* 1999; **81**: 1344–50.
9 Melotti A, Daga A, Marubbi D, Zunino A, Mutti L, Corte G. *In vitro* and *in vivo* characterization of highly purified human mesothelioma derived cells. *BMC Cancer* 2010; **10**: 54.
10 Nakataki E, Yano S, Matsumori Y *et al.* Novel orthotopic implantation model of human malignant pleural mesothelioma (EHMES-10 cells) highly expressing vascular endothelial growth factor and its receptor. *Cancer Sci* 2006; **97**: 183–91.
11 Martarelli D, Catalano A, Procopio A, Orecchia S, Libener R, Santoni G. Characterization of human malignant mesothelioma cell lines orthotopically implanted in the pleural cavity of immunodeficient mice for their ability to grow and form metastasis. *BMC Cancer* 2006; **6**: 130.

doi: 10.1111/j.1349-7006.2010.01827.x

12 Yanagihara K, Tsumuraya M, Takigahira M *et al.* An orthotopic implantation mouse model of human malignant pleural mesothelioma for *in vivo* photon counting analysis and evaluation of the effect of S-1 therapy. *Int J Cancer* 2010; **126**: 2835–46.
13 Addis B, Roche H. Problems in mesothelioma diagnosis. *Histopathology* 2009; **54**: 55–68.
14 Husain AN, Colby TV, Ordonez NG *et al.* Guidelines for pathologic diagnosis of malignant mesothelioma: a consensus statement from the International Mesothelioma Interest Group. *Arch Pathol Lab Med* 2009; **133**: 1317–31.
15 Sato A, Torii I, Okamura Y *et al.* Immunocytochemistry of CD146 is useful to discriminate between malignant pleural mesothelioma and reactive mesothelium. *Mod Pathol* 2010; **23**: 1458–66.
16 Whitaker D, Henderson DW, Shilkin KB. The concept of mesothelioma *in situ*: implications for diagnosis and histogenesis. *Semin Diagn Pathol* 1992; **9**: 151–61.
17 Henderson DW, Shilkin KB, Whitaker D. Reactive mesothelial hyperplasia vs mesothelioma, including mesothelioma *in situ*: a brief review. *Am J Clin Pathol* 1998; **110**: 397–404.
18 Churg A, Colby TV, Cagle P *et al.* The separation of benign and malignant mesothelial proliferations. *Am J Surg Pathol* 2000; **24**: 1183–200.
19 Cagle PT, Churg A. Differential diagnosis of benign and malignant mesothelial proliferations on pleural biopsies. *Arch Pathol Lab Med* 2005; **129**: 1421–7.
20 Stevens MW, Leong AS, Fazzalari NL, Dowling KD, Henderson DW. Cytopathology of malignant mesothelioma: a stepwise logistic regression analysis. *Diagn Cytopathol* 1992; **8**: 333–41.
21 Whitaker D. The cytology of malignant mesothelioma. *Cytopathology* 2000; **11**: 139–51.
22 Kushitani K, Takeshima Y, Amatya VJ, Furonaka O, Sakatani A, Inai K. Differential diagnosis of sarcomatoid mesothelioma from true sarcoma and sarcomatoid carcinoma using immunohistochemistry. *Pathol Int* 2008; **58**: 75–83.
23 Onofre FB, Onofre AS, Pomjanski N, Buckstegge B, Grote HJ, Bocking A. 9p21 Deletion in the diagnosis of malignant mesothelioma in serous effusions additional to immunocytochemistry, DNA-ICM, and AgNOR analysis. *Cancer* 2008; **114**: 204–15.
24 Yokoyama T, Osada H, Murakami H *et al.* YAP1 is involved in mesothelioma development and negatively regulated by Merlin through phosphorylation. *Carcinogenesis* 2008; **29**: 2139–46.
25 Hassan R, Ho M. Mesothelin targeted cancer immunotherapy. *Eur J Cancer* 2008; **44**: 46–53.
26 Feng Y, Xiao X, Zhu Z *et al.* A novel human monoclonal antibody that binds with high affinity to mesothelin-expressing cells and kills them by antibody-dependent cell-mediated cytotoxicity. *Mol Cancer Ther* 2009; **8**: 1113–8.
27 Inamoto T, Yamada T, Ohnuma K *et al.* Humanized anti-CD26 monoclonal antibody as a treatment for malignant mesothelioma tumors. *Clin Cancer Res* 2007; **13**: 4191–200.
28 Bidlingmaier S, He J, Wang Y *et al.* Identification of MCAM/CD146 as the target antigen of a human monoclonal antibody that recognizes both epithelioid and sarcomatoid types of mesothelioma. *Cancer Res* 2009; **69**: 1570–7.

Gen Thorac Cardiovasc Surg (2011) 59:61–64
DOI 10.1007/s11748-010-0600-4

CASE REPORT

Intrapulmonary solitary fibrous tumor

Koji Kawaguchi, MD · Tetsuo Taniguchi, MD
Noriyasu Usami, MD · Kohei Yokoi, MD

Received: 1 November 2009 / Accepted: 11 February 2010

Abstract Solitary pulmonary nodules are sometimes detected by routine chest radiography. Although many of them are suspected to be benign tumors following noninvasive examinations including computed tomography and positron emission tomography, it is difficult to diagnose them accurately. This report presents a rare case of a solitary fibrous tumor located in the lung that could not be diagnosed preoperatively. More information must be accumulated concerning such rare cases of intrapulmonary solitary fibrous tumors.

Key words Pulmonary nodule · Solitary fibrous tumor · Surgery

Introduction

Asymptomatic solitary pulmonary nodules are sometimes detected by routine chest radiography. Although imaging modalities, including positron emission tomography (PET), are available and make it easier to diagnose such tumors, it is still difficult to provide a precise diagnosis of a benign tumor of the lung.[1] Many of these pulmonary benign tumors cannot be definitively diagnosed preoperatively.

Solitary fibrous tumors (SFTs) are spindle cell neoplasms and predominantly originate from the pleura.[2] The tumors are usually attached to the pleura by pedicles and hence may show different positions within the pleural surface on serial radiographs. This specific radiographic finding might be helpful to diagnose SFTs; however, tumors that arise at unusual sites often go unrecognized or misdiagnosed.[3] This report presents a rare case of an SFT located in the lung. We also review the relevant literature.

K. Kawaguchi (✉) · T. Taniguchi · N. Usami · K. Yokoi
Division of Thoracic Surgery, Nagoya University Graduate School of Medicine, 65 Tsurumai-cho, Showa-ku, Nagoya 466-8550, Japan
Tel. +81-52-744-2376; Fax +81-52-744-2383
e-mail: gucci@med.nagoya-u.ac.jp

Case report

A 60-year-old woman was referred to our institution because of an abnormal nodule detected in her left lung. It had at first been detected 2 years earlier and had since increased in its largest dimension from 2 cm to 3 cm on her chest roentgenograms (Fig. 1). She had no history of cough, sputum, shortness of breath, or smoking. Computed tomography (CT) scans revealed a well-circumscribed nodule measuring 23 mm without calcification and spicula in the left S3 segment of the lung close to the mediastinum (Fig. 2). The nodular lesion was strongly contrasted at the late phase of an enhanced CT scan. PET using ^{18}F-fluorodeoxyglucose exhibited little uptake in the lesion [the maximum standard uptake value (SUVmax) was 1.62]. Other examinations, including serum tumor markers, showed no abnormalities.

She underwent a thoracotomy because the lesion was suspected to be either a benign tumor or a low-grade malignant tumor. The mass was found in the pulmonary parenchyma without involving the pleural surface. A needle biopsy was performed, and a low-grade malignant tumor was suggested from the frozen sections. A left upper segmentectomy was therefore performed with mediastinal lymph node sampling.

Macroscopically, the resected tumor, which measured 23 × 22 × 19 mm, was firm and ovoid. The cross section

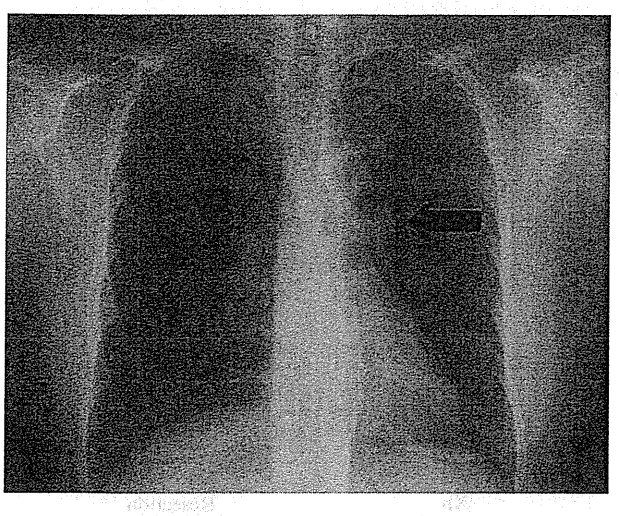

Fig. 1 Chest roentgenogram (posteroanterior view). A well-circumscribed nodule (*arrow*) was detected in the left hilum of the thorax

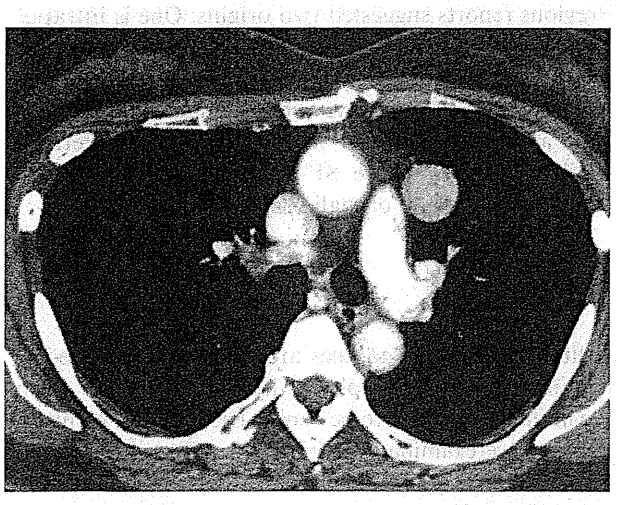

Fig. 2 Computed tomography (CT) scan. The nodular lesion in the left S3 segment of the lung was strongly contrasted at the late phase of an enhanced CT scan

was solid, grayish-white, and well circumscribed without involving the visceral pleura (Figs. 3, 4A). The pathologic examination revealed that the tumor consisted of proliferating spindle cells with a random fascicular arrangement, which were separated by variable amounts of wavy hyalinized collagen (Fig. 4B). The tumor cells exhibited a positive reaction for CD34 and a negative reaction for calretinin, smooth muscle actin, and S-100 by immunohistochemistry. The MIB-1 index was 2%–3%.

The final diagnosis was an intrapulmonary benign SFT. The patient was well with no apparent tumor recurrence at 6 months after the operation.

Discussion

The SFT is a localized pleural neoplasm first described in 1931.[4] The origin of this tumor is currently recognized as submesothelial cells, and most of these tumors arise

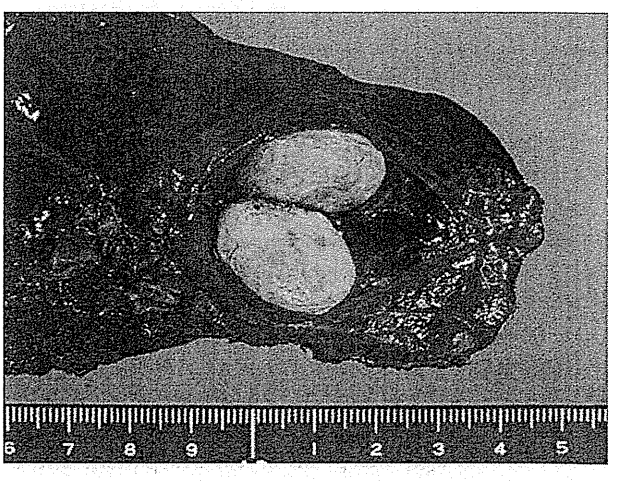

Fig. 3 Gross appearance of the resected specimen. The cross section was a solid, grayish-white, well-circumscribed mass that did not involve the visceral pleura

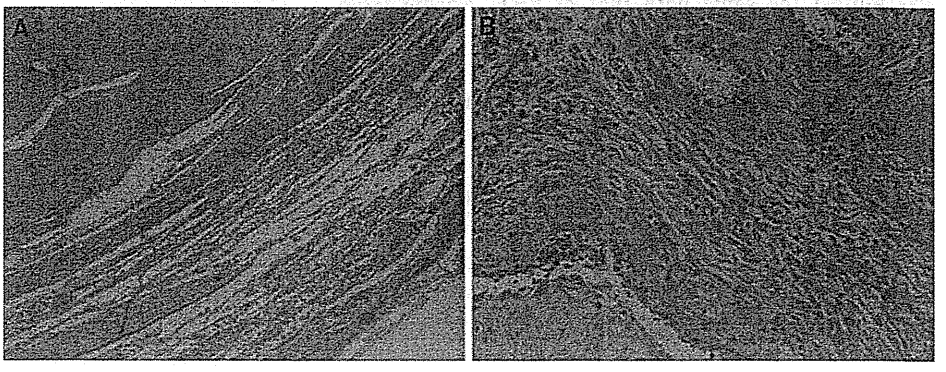

Fig. 4 Pathological findings in the tumor. **A** The tumor appeared distinct from the visceral pleura (H&E, ×40). **B** Proliferating spindle cells with a random fascicular arrangement were observed with the deposition of wavy hyalinized collagen (H&E, ×200)

Table 1 Reported cases of intrapulmonary solitary fibrous tumors in the English-language literature

Study	Year	Age/sex	Size (mm)	Test or finding	Treatment
Yousem[6]	1988	71 M	35	Xp	Resection
		55 F	15	Cough	Resection
		82 F	30	Cough	Resection
Goodlad[3]	1991	55 M	15	Arthralgia	Resection
		60 M	6	OAP	Resection
van de Rijn[7]	1994	69 M	120	Unknown	Discovered at autopsy
		80 F	Unknown	Unknown	Resection
Aufiero[8]	1995	20 F	30	Xp	Resection
Caruso[9]	1996	72 M	60	Xp	Resection
Kahlifa[10]	1997	68 F	27	Xp	Resection
Chan[11]	1999	73 F	30	Xp	Resection
Kanamori[12]	2005	8 M	45	Fever	Resection
Baliga[13]	2007	42 M	120	Unknown	Ablation
Sagawa[14]	2007	72 F	12	Xp	Resection
Sakurai[15]	2008	45 M	22	Xp	Resection
Present case	2010	60 F	23	Xp	Resection

OAP, osteoarthropathy; Xp. chest roentgenography

from the pleura. Approximately 10%–37% of them show malignant features based on nuclear atypia, necrosis, more than four mitoses per 10 high-power fields, and clinical behavior.[2,5] The best and most reliable treatment is complete resection for both benign and malignant SFTs.

There are a few reports of SFTs arising at unusual sites, including the lung, peritoneum, thyroid, and nasal cavity, among others. The World Health Organization currently defines SFT as a mesenchymal neoplasm, and this tumor might also be found at other locations.

A review of the literature revealed 11 English-language reports including 15 cases of the SFT located in the lung, shown in Table 1. The tumors were distributed evenly between the sexes and were found during middle to old age, except an 8-year-old patient and a 20-year-old patient. About half of the lesions were incidentally detected by routine chest roentgenography; the others were found because of their symptoms including cough, sputum, dyspnea, arthralgia, and osteoarthropathy. The ratio of patients with or without symptoms was almost the same with that of SFTs arising from the pleura.

Complete resection was the sole curative procedure for intra- and extrapulmonary SFTs. The type of lung resection was determined by the size and location of the tumor; a segmentectomy was chosen in the current case because a low-grade malignant tumor was suspected based on frozen sections from the intraoperative fine-needle biopsy specimen. Among the previous reports, none of SFTs located in the lung was diagnosed as malignant with one exception in a Japanese case report.[16]

The reason SFTs arise entirely in the lung is unclear. Previous reports suggested two origins: One is intrapulmonary, with entrapped cells from the pleura; and the other is the lung parenchyma itself. It is difficult to solve this mystery, although we did recognize that patients with an SFT located in the lung had characteristics similar to those whose SFTs arose from the pleura (except for the ratio of malignant cases).

Conclusion

Solitary pulmonary nodules are sometimes detected by routine chest radiography. Although many of them are initially suspected to be benign based on the results of noninvasive examinations including CT and PET, it is difficult to diagnose them accurately. It is therefore important to be aware that rare cases of SFT located in the lung are occasionally encountered in clinical practice.

References

1. Wahidi MM, Govert JA, Goudar RK, Gould MK, McCrory DC. Evidence for the treatment of patients with pulmonary nodules: when is it lung cancer? ACCP evidence-based clinical practice guidelines (2nd edition). Chest 2007;132:94S–107S.
2. England DM, Hochholzer L, McCarthy MJ. Localized benign and malignant fibrous tumors of the pleura: a clinicopathologic review of 223 cases. Am J Surg Pathol 1989;13:640–58.
3. Goodlad JR, Fletcher CD. Solitary fibrous tumour arising at unusual sites: analysis of a series. Histopathology 1991;19:515–22.
4. Klemperer P, Rabin LB. Primary neoplasms of the pleura. Arch Pathol 1931;11:385–412.

5. Vallat-Decouvelaere AV, Dry SM, Fletcher CD. Atypical and malignant solitary fibrous tumors in extrathoracic locations: evidence of their comparability to intra-thoracic tumors. Am J Surg Pathol 1998;22:1501–11.
6. Yousem SA, Flynn SD. Intrapulmonary localized fibrous tumor. Intraparenchymal so-called localized fibrous mesothelioma. Am J Clin Pathol 1988;89:365–9.
7. van de Rijn M, Lombard CM, Rouse RV. Expression of CD34 by solitary fibrous tumors of the pleura, mediastinum, and lung. Am J Surg Pathol 1994;18:814–20.
8. Aufiero TX, McGary SA, Campbell DB, Phillips PP. Intrapulmonary benign fibrous tumor of the pleura. J Thorac Cardiovasc Surg 1995;110:549–51.
9. Caruso RA, LaSpada F, Gaeta M, Minutoli I, Inferrera C. Report of an intrapulmonary solitary fibrous tumor: Fine-needle aspiration cytologic findings, clinicopathological, and immunohistochemical features. Diagn Cytopathol 1996;14: 64–7.
10. Khalifa MA, Montgomery EA, Azumi N, Gomes MN, Zemar RK, Min KW, Lack EE. Solitary fibrous tumors: a series of lesions, some in unusual sites. South Med J 1997;90:793–9.
11. Chang YL, Lee YC, Wu CT. Thoracic solitary fibrous tumor: clinical and pathological diversity. Lung Cancer 1999;23:53–60.
12. Kanamori Y, Hashizume K, Sugiyama M, Motoi T, Fukayama M, Ida K, Igarashi T. Intrapulmonary solitary fibrous tumor in an eight-year-old male. Pediatr Pulmonol 2005;40:261–4.
13. Baliga M, Flowers R, Heard K, Siddiqi A, Akhtar I. Solitary fibrous tumor of the lung: a case report with a study of the aspiration biopsy, histopathology, immunohistochemistry, and autopsy findings. Diagn Cytopathol 2007;35:239–44.
14. Sagawa M, Ueda Y, Matsubara F, Sakuma H, Yoshimitsu Y, Aikawa H, Usuda K, Minato H, Sakuma T. Intrapulmonary solitary fibrous tumor diagnosed by immunohistochemical and genetic approaches: report of a case. Surg Today 2007;37: 423–5.
15. Sakurai H, Tanaka W, Kaji M, Yamazaki K, Suemasu K. Intrapulmonary localized fibrous tumor of the lung: a very unusual presentation. Ann Thorac Surg 2008;86:1360–2.
16. Aoshima H, Oyama K, Ikeda T, Murasugi M, Oniuki T, Sawada T. A case of intrapulmonary malignant solitary fibrous tumor with abnormal uptake on FDG-PET. Jpn J Lung Cancer 2008;48:51–5.

Original Paper

Cellular Physiology and Biochemistry

Cell Physiol Biochem 2012;29:241-250

Accepted: November 28, 2011

PDGF-D/PDGF-ββ Receptor-Regulated Chemotaxis of Malignant Mesothelioma Cells

Asuka Okada[1,2*], Takahiro Yaguchi[1*], Takeshi Kanno[1], Akinobu Gotoh[3], Takashi Nakano[2] and Tomoyuki Nishizaki[1]

[1]Division of Bioinformation, Department of Physiology, Hyogo College of Medicine, Nishinomiya, [2]Department of Thoracic Oncology, Hyogo College of Medicine, Nishinomiya, [3]Laboratory of Cell and Gene Therapy, Institute for Advanced Medical Sciences, Hyogo College of Medicine, Nishinomiya, *A. Okada and T. Yaguchi contributed equally to this work

Key Words

Malignant mesothelioma cell • Chemotaxis • PDGF-ββ receptor • ROCK • ERK

Abstract

Background/Aims:Our earlier study suggested that platelet-derived growth factor (PDGF)-ββ receptor regulates chemotaxis of human malignant mesothelioma cells such as MSTO-211H, NCIH-2052, NCIH-2452, and NCIH-28 cells, but not non-malignant Met5A cells. The present study was designed to gain further insight into the PDGF-ββ receptor signals underlying the chemotaxis. Methods: PDGF-D secreted from cells, activation of Akt and ERK, and cell migration were monitored for cells with and without knocking-down PDGF-ββ receptor. Results: FBS significantly stimulated PDGF-D secretion from malignant mesothelioma cells, but not Met5A cells. PDGF-D activated Akt and ERK in both the non-malignant and malignant cells. PDGF-D significantly facilitated migration of malignant mesothelioma cells, but not Met5A cells, with the extent varying among the cell types. The facilitatory action of PDGF-D was clearly prevented by knocking-down PDGF-ββ receptor or inhibitors of PI3 kinase, PDK1, Akt, Rac1, ROCK, and MEK. Conclusion: The results of the present study indicate that PDGF-D promotes malignant mesothelioma cell chemotaxis through PDGF-ββ receptor signaling pathways along a PI3 kinase/PDK1/Akt/Rac1/ROCK axis and relevant to ERK activation.

Introduction

Malignant mesothelioma, originated from mesothelial cells, is a locally aggressive and highly lethal tumor, that is caused by exposure to asbestos [1]. Malignant mesotheliomas are characterized by rapid and diffuse invasion into the peritoneum through the diaphragm or the pleura through the mediastinum. Mesothelioma cells express a variety of growth factors including platelet-derived growth factor (PDGF), that act in an autocrine manner [2, 3]. PDGFs such as PDGF-A, -B, -C and -D regulate cell growth and chemotaxis both in cancer cells and normal cells [4]. Higher expression of PDGF-A and

KARGER

Fax +41 61 306 12 34
E-Mail karger@karger.ch
www.karger.com

1015-8987/12/0292-0241$38.00/0

Accessible online at:
www.karger.com/cpb

Prof. Tomoyuki Nishizaki
Division of Bioinformation, Department of Physiology,
Hyogo College of Medicine, 1-1 Mukogawa-cho, Nishinomiya 663-8501 (Japan)
Tel. +81-798-45-6397, Fax +81-798-45-6649
E-Mail tomoyuki@hyo-med.ac.jp

-B is found with lung and pleural tumors [5]. PDGF-A and -B are extracellularly secreted from malignant mesothelioma cells [6-8]. PDGF-A plays a role in mesothelial tumor initiation at early stages [9] and PDGF-B acts as a chemoattractant for malignant mesothelioma [10, 11].

PDGF-A and -B are secreted as active dimers composed of single-domain protein chains (PDGF-AA and -BB), but otherwise, PDGF-C and -D, containing an N-terminal CUB and a conserved C-terminal growth factor domain, are secreted as a latent dimeric factor and undergo proteolytic processing at the hinge region between the CUB domain and the growth factor domain, to produce active form of PDGF-CC and -DD [12-14]. PDGF receptors consist of the PDGF-α and/or -β subunit such as αα homodimer, αβ heterodimer, and ββ homodimer [12]. PDGF-αα and -αβ receptors are activated by PDGF-AA, -BB, and -CC, and PDGF-ββ is activated by PDGF-DD [12-14].

Evidence has pointed to significance of PDGF-D in tumor development and progression [15]. Urokinase plasminogen activator (uPA), that forms the active dimer PDGF-DD through extracellular proteolytic processing, contributes to progression of prostate cancer [16, 17]. Conversely, urinary trypsin inhibitor (UTI), a potent inhibitor of uPA, is capable of preventing metastasis in a variety of cancer cells [18-23]. In our earlier study, UTI inhibited fetal bovine serum (FBS)-induced migration of human malignant mesothelioma cells [24]. This suggests that PDGF-D, undergoing uPA-mediated proteolytic processing, promotes malignant mesothelioma cell chemotaxis through a PDGF-ββ receptor signaling pathway.

The present study was conducted to obtain direct evidence for PDGF-D/PDGF-ββ receptor-regulated chemotaxis of malignant mesothelioma cells. We show here that PDGF-D promotes malignant mesothelioma cell chemotaxis by activating phosphoinositide 3-kinase (PI3 kinase), phosphoinositide-dependent kinase-1 (PDK1), Akt, Rac1, and Rho-associated coiled-coil forming protein kinase (ROCK) or extracellular signal-regulated kinase (ERK) as mediated via PDGF-ββ receptors.

Materials and Methods

Cell culture

Human malignant mesothelioma cell lines such as MSTO-211H, NCIH-2052, NCIH-2452, and NCIH-28 cells and the human non-malignant mesothelial cell line, Met5A cells, were purchased from American Type Culture Collection (Manassas, VA, USA). Cells were grown in RPMI-1640 medium supplemented with 10% heat-inactivated FBS, 0.003% L-glutamine, penicillin (final concentration, 100 U/ml), and streptomycin (final concentration, 0.1 mg/ml), in a humidified atmosphere of 5% CO_2 and 95% air at 37 °C.

Monitoring of PDGF-D secretion

Cells were untreated and treated with 1% (v/v) FBS for 24 h, and extracellular culture medium was collected. The medium was incubated with an anti-PDGF-D antibody (1 μg) (R&D systems, Minneapolis, MN, USA) at 4 °C for 24 h, and subsequently, 20 μl of protein G agarose (GE healthcare, Piscataway, NJ, USA) was added followed by further incubation at 4 °C for 24 h by continuously shaking. After centrifugation at 3,000 rpm for 1 min, the pellets were washed twice with Tris Buffered Saline with Tween 20 (TBST)[150 mM NaCl, 0.1% (v/v) Tween20, and 20 mM Tris, pH 7.5] and dissolved in 40 μl of a sodium dodecyl sulfate (SDS)-polyacrylamide sample buffer [0.2 mM Tris-HCl, 0.04% (w/v) SDS, 20% (v/v) glycerol, pH 6.8]. After boiling at 100 °C for 5 min, proteins were separated by 12% (w/v) SDS-polyacrylamide gel electrophoresis (SDS-PAGE), and transferred to polyvinylidene fluoride (PVDF) membranes. Blotting membranes were blocked with 5% (w/v) bovine serum albumin (BSA) and reacted with an anti-PDGF-D antibody (1:1000)(R&D systems), followed by a horseradish peroxidase (HRP)-conjugated anti-goat IgG antibody (1:5000)(MP Biomedicals Inc., Ohio, USA). Immunoreactivity was detected with an enhanced chemiluminescence (ECL) kit (GE Healthcare) and visualized with an Image Gauge software (FUJIFILM, Tokyo, Japan). The amount of PDGF-D secretion was normalized by regarding immunoreactive signals before FBS treatment as 1.

Knocking-down PDGF-ββ receptor

Small interfering RNAs (siRNAs) silencing the PDGF receptor β subunit-targeted gene (PDGF-βR siRNA): sense, 5'-GGA AUG AGG UGG UCA ACU UTT-3' and anti-sense, 5'-AAG UUG ACC ACC UCA UUC CTT-3'; sense, 5'-GCU CAU GGC CUG AGC CAU UTT- 3' and anti-sense, 5'-A AUG GCU CAG GCC AUG AGC TT-3'; and sense, 5'-GAG AGG ACC UGC CGA GCA ATT-3' and anti-sense, 5'-UUG CUC GGC AGG UCC UCU CTT-3', and negative control siRNA (NC siRNA) were purchased from Santa Cruz Biotechnology (Santa Cruz, CA, USA). siRNAs were transfected using Lipofectamine LTX (Invitrogen, Carlsbad, CA, USA).

Chemotaxis assay

Cell migration was monitored with an EZ-TAXIScan (Effector Cell Institute, Piscataway, NJ, USA) equipped with a 6-channel chamber by the method as previously described [24]. Briefly, cells (5 x 10^6 cells/ml), transfected with the NC siRNA or the PDGF-βR siRNA, were seeded into a hole (1 mm^3 in volume) in a KK-chamber filled with RPMI-HEPES medium at 37 °C, aspirated from the opposite side, to come out from the hole, and lined up on the plate to adjust the starting grid. Subsequently, PDGF (4 ng) together with and without a variety

of inhibitors was applied into another hole (1 mm^3 in volume) located on the opposite side of the chamber. Cell mobilizations were detected at 3-min intervals through a high performance lens connected to a CCD camera with a coaxial episcopic illumination system, and analyzed with a developed using a C^{++} Builder 6 software (Borland, CA, USA). The migratory pathway was recorded by clicking each cell on a display.

Reverse transcription-polymerase chain reaction (RT-PCR)

Total RNAs were purified from cells, transfected with and without the NC siRNA or the PDGF-βR siRNA, by an acid/guanidine/thiocyanate/chloroform extraction method using a Sepasol-RNA I Super kit. After purification, total RNAs were treated with RNase free-DNase I (2 unit) at 37 °C for 30 min to remove genomic DNAs, and 10 μg of RNAs were resuspended in water. Then, oligo dT primers, dNTPs, 5 x First Strand buffer, and SuperScripit III RNase H-Reverse Transcriptase were added to the RNA solution and incubated at 65 °C for 5 min followed by 56 °C for 60 min, 58 °C for 60 min, 85 °C for 5 min to synthesize the first strand cDNA. Subsequently, 1 μl of the reaction solution was diluted with water and mixed with 10 x PCR reaction buffer, dNTPs, $MgCl_2$, oligonucleotide, dimethylsulfoxide [final concentration, 5% (v/v)] and 1 unit of Taq polymerase (Fermentas, St. Leon-Roth, Germany)(final volume, 20 μl). RT-PCR was carried out with a GeneAmp PCR system model 9600 DNA thermal cycler (Applied Biosystems, Indianapolis, IN, USA) programmed as follows: the first one step, 94 °C for 4 min and the ensuing 30 cycles, 94 °C for 1 s, 62 °C for 15 s, and 72 °C for 30 s. The primers used here were as follows: sense, 5'-CGA GTG GAC ATA CCC CCG CAA-3' and anti-sense, 5'-CAG CAC TCG GAC AGG GAC ATT GAT-3' for the PDGF receptor β subunit and sense, 5'-GAC TTC AAC AGC GAC ACC CAC TCC-3' and anti-sense, 5'-AGG TCC ACC ACC CTG TTG CTG TAG-3' for GAPDH. PCR products were stained with ethidium bromide and visualized by 2% (w/v) agarose gel electrophoresis.

Monitoring activation of Akt and ERK

Cells, transfected with the NC siRNA or the PDGF-βR siRNA, were treated with PDGF-D for 10 min, and then lysed in a lysate solution [150 mM NaCl, 20 mM Tris, 0.1% (v/v) Tween-20 and 0.1% (w/v) SDS, pH 7.5] containing 1% (v/v) protease inhibitor cocktail and 1% (v/v) phosphatase inhibitor cocktail, and then centrifuged at 3,000 rpm for 5 min at 4 °C. Proteins were separated by SDS-PAGE using a TGX gel (BioRad, Hercules, CA, USA) and then transferred to PVDF membranes. Blotting membranes were blocked with TBST containing 5% (w/v) bovine serum albumin and subsequently reacted with an anti-pAkt (Thr308) antibody (Cell Signaling, Beverly, MA, USA), an anti-Akt antibody (Cell Signaling), an anti-pERK antibody (Santa Cruz), an anti-ERK antibody (Santa Cruz), or an anti-β-actin antibody (Sigma, St Louis, MO, USA). After washing, membranes were reacted with a horseradish peroxidase-conjugated goat anti-mouse IgG or goat anti-rabbit IgG antibody. Immunoreactivity was detected with an ECL kit (GE Healthcare) and visualized using a chemiluminescence detection system (GE Healthcare). Protein concentrations for each sample were determined with a BCA protein assay kit (Thermo Fisher Scientific, Waltham, MA, USA).

Statistical analysis

Statistical analysis was carried out using unpaired *t*-test and Dunnett's test.

Results

FBS stimulates PDGF-D secretion from malignant mesothelioma cells

We have earlier found that the uPA inhibitor UTI inhibited FBS-induced migration of human malignant mesothelioma cells [24]. This, in the light of the fact that an active form of PDGF-D is produced through uPA-mediated proteolytic processing, raises the possibility that FBS stimulates PDGF-D secretion to activate PDGF-ββ receptors, responsible for malignant mesothelioma cell chemotaxis. To obtain evidence for this, we initially monitored PDGF-D secretion from malignant mesothelioma cells.

Human non-malignant Met5A mesothelial cells and malignant mesothelioma cells such as MSTO-211H, NCIH-2052, NCIH-2452, and NCIH-28 cells were cultured in the presence and absence of 1% (v/v) FBS for 24 h. Then, extracellular culture medium was collected and immunoprecipitated with an anti-PDGF-D antibody. Immunoprecipitants were subjected to SDS-PAGE followed by Western blotting using an anti-PDGF-D antibody, to detect PDGF-D extracellularly secreted. For MSTO-211H, NCIH-2052, NCIH-2452, and NCIH-28 cells, FBS significantly increased the amount of extracellular PDGF-D to a variety of extents ranging from 1.5 to 3 folds of basal levels, depending upon cell types, while no significant increase was obtained with non-malignant Met5A cells (Fig. 1). This indicates that FBS stimulates PDGF-D secretion from malignant mesothelioma cells, but not non-malignant cells.

PDGF-D promotes malignant mesothelioma cell chemotaxis in a PDGF-ββ receptor-dependent manner

PDGF receptors include PDGF-αα, -αβ, and ββ receptors, and PDGF-D is an agonist of PDGF-ββ receptor. Then, we thought that PDGF-D might regulate malignant mesothelioma cell chemotaxis by targeting PDGF-ββ receptor. To address this question, we constructed the siRNA silencing the PDGF receptor β

subunit-targeted gene. Expression of the PDGF-β subunit mRNA was clearly suppressed for cells transfected with the PDGF-βR siRNA as compared with the expression for cells transfected with the NC siRNA (Fig. 3A). This confirms knocking-down of PDGF-ββ receptor for cells transfected with the PDGF-βR siRNA.

We next monitored cell migration using an EZ-TAXIScan (Fig. 2). For malignant mesothelioma cells such as MSTO-211H, NCIH-2052, NCIH-2452, and NCIH-28 cells transfected with the NC siRNA, PDGF-D facilitated migration, with the different potency among cell types (Fig. 3B). The facilitatory action of PDGF-D was significantly prevented by knocking-down PDGF-ββ receptor (Fig. 3B). In contrast, PDGF-D did not facilitate migration of non-malignant Met5A cells transfected with the NC siRNA, and the migration was not affected by knocking-down PDGF-ββ receptor (Fig. 3B). It is indicated from these results that PDGF-D promotes migration of malignant mesothelioma cells, but not non-malignant cells, by activating PDGF-ββ receptor.

PDGF-D promotes malignant mesothelioma cell migration by activating PI3 kinase, PDK1, Akt, Rac1, and ROCK or ERK as mediated via PDGF-ββ receptors

PDGF-ββ receptor as well as other growth factor receptors would be linked to two major signaling pathways: one is a pathway along a PI3 kinase/PDK1/Akt/Rac1 (Cdc42)/ROCK axis and another is a pathway along a Ras/Raf/MAP kinase kinase kinase (MEKK)/MAP kinase kinase (MEK)/MAP kinase (MAPK) axis (Fig. 4). To ascertain the implication of PDGF-ββ receptor in those signaling pathways, we examined activation of Akt and ERK, a MAPK, in cells with and without knocking-down of PDGF-ββ receptor. Akt is phosphorylated and activated by PDK1. ERK is phosphorylated and activated by MEK. In the Western blot analysis, PDGF-D increased phosphorylated Akt for all the non-malignant and malignant mesothelioma cells used here, and the effect was significantly attenuated by knocking-down PDGF-ββ receptor (Fig. 5A-E), indicating that PDGF-D actually activates Akt in non-malignant and malignant mesothelioma cells via PDGF-ββ receptors. This also suggests that Akt is activated as a downstream effector of PDK1 in a PDGF-ββ receptor/PI3 kianse/PDK1/Akt/Rac1/ROCK pathway.

For ERK, immunoreactive signals against an anti-ERK-antibody were detected at 42 and 44 kDa, which correspond to ERK2 and ERK1, respectively (Fig. 5A-E). PDGF-D increased phosphorylated ERK at 44 kDa

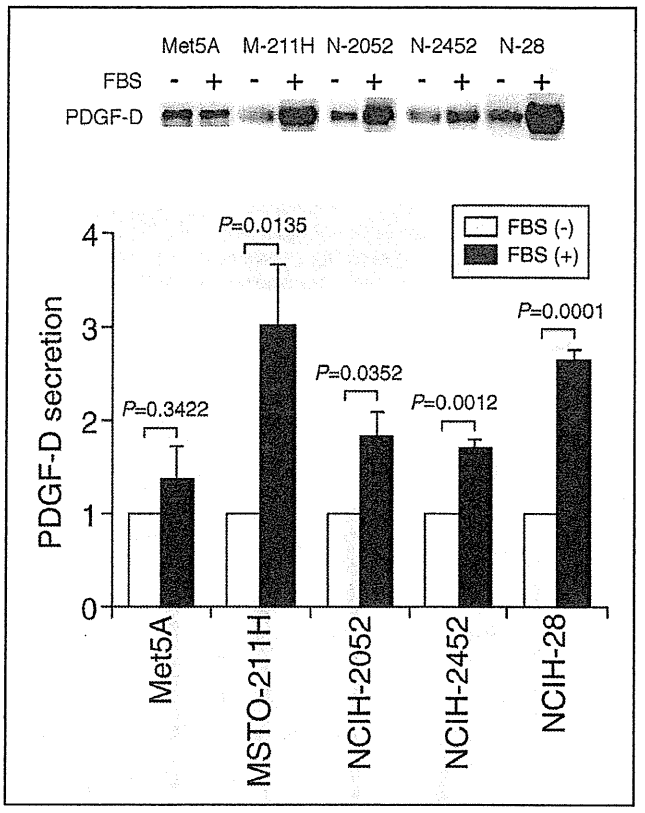

Fig. 1. PDGF-D secretion from non-malignant and malignant mesothelioma cells. Culture medium for Met5A, MSTO-211H, NCIH-2052, NCIH-2452, and NCIH-28 cells was collected after 24-h non-treatment and treatment with 1% (v/v) FBS and immunoprecipitated with an anti-PDGF-D antibody followed by Western blotting using an anti-PDGF-D antibody. The ratio of the PDGF-D immunoreactive signal intensity for FBS-treated samples against the intensity for FBS-untreated samples was calculated. In the graph, each value represents the mean (± SEM) relative intensity (n=3 independent experiments). *P* values, unpaired *t*-test.

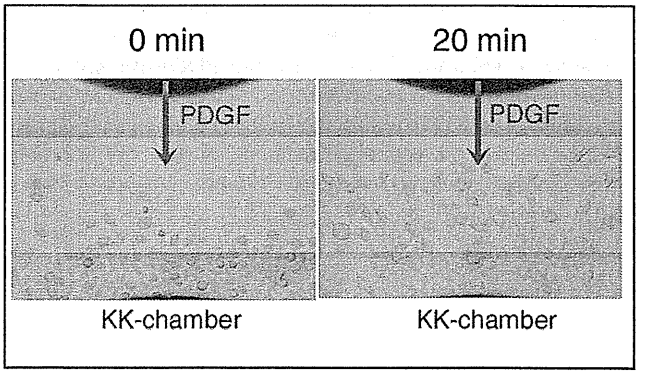

Fig. 2. Chemotaxis monitoring. Cells were seeded in a KK-chamber. PDGF-D (4 ng) was applied into a hole located on the opposite side of the chamber, and cell mobilizations were monitored for 20 min. Cells shown here are NCIH-2052 cells. Note that cells move towards PDGF-D at 20 min.

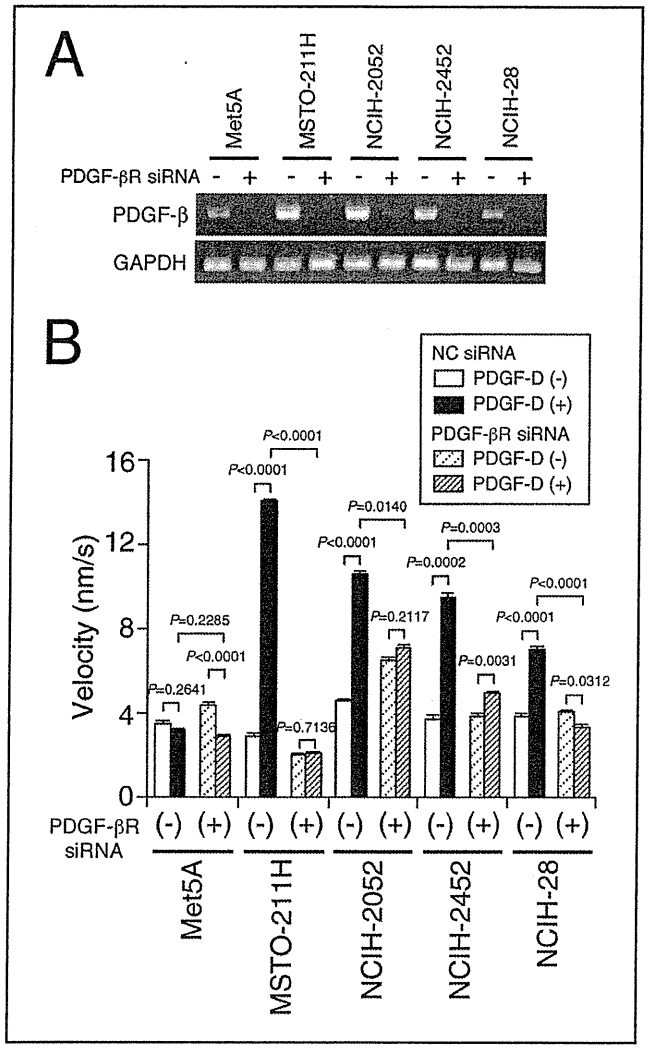

Fig. 3. PDGF-D-induced facilitation of malignant mesothelioma cell chemotaxis as mediated via PDGF-ββ receptors. (A) Cells as indicated were transfected with the NC siRNA [PDGF-βR siRNA (-)] or the PDGF-βR siRNA [PDGF-βR siRNA (+)], and RT-PCR was carried out (n=3 independent experiments). Note that no signal band for the PDGF receptor β subunit mRNA is visible in cells transfected with the PDGF-βR siRNA. (B) Chemotaxis assay was carried out in cells transfected with the NC siRNA or the PDGF-βR siRNA by applying PDGF-D (4 ng). In the graph, each value represents the mean (± SEM) velocity (n=15 independent experiments). *P* values, unpaired *t*-test.

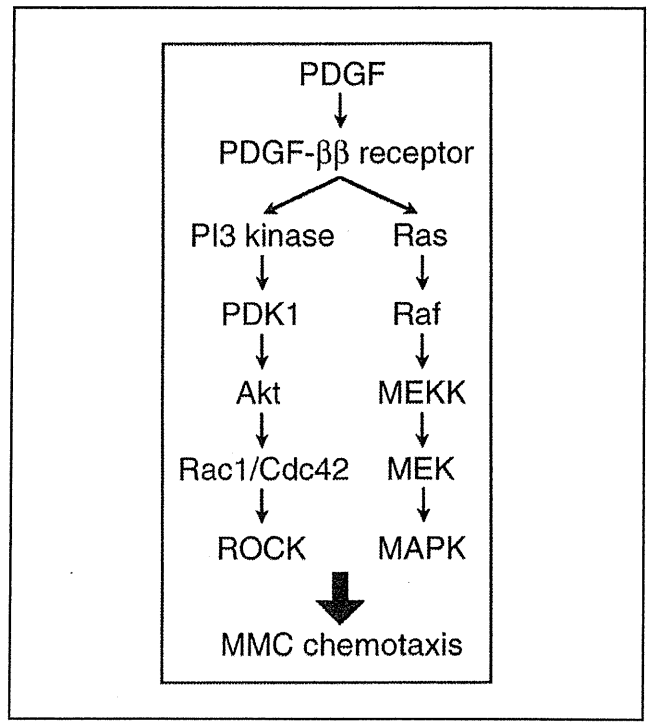

Fig. 4. Schematic diagram for PDGF-D/PDGF-ββ receptor signaling pathways. MMC, malignant mesothelioma cell.

for all the non-malignant and malignant mesothelioma cells, and the effect was significantly inhibited by knocking-down PDGF-ββ receptor (Fig. 5A-E), indicating that PDGF-D activates ERK1 in mesothelioma cells via PDGF-ββ receptors. This also suggests that ERK1 is activated as a downstream effector of MEK in a PDGF-ββ receptor/Ras/Raf/MEKK/MEK/MAPK pathway.

Our final attempt was to see whether malignant mesothelioma cell chemotaxis is regulated through those pathways. PDGF-D promoted migration of all the malignant mesothelioma cells used here, with the different potency among cell types, and the effect was abolished by the PI3 kinase inhibitor wortmannin, although PDGF-D had no effect on Met5A cell migration in the presence and absence of wortmannin (Fig. 6A). This indicates the participation of PI3 kinase, a downstream effector of PDGF-ββ receptor, in PDGF-D-engaged regulation of malignant mesothelioma cell migration.

PDGF-D-induced facilitation of malignant mesothelioma cell migration was clearly prevented by the PDK1 inhibitor BX912, while Met5A cell migration was not affected by PDGF-D in the presence and absence of BX912 (Fig. 6B). This indicates the participation of PDK1, a downstream effector of PI3 kinase, in PDGF-D-engaged regulation of malignant mesothelioma cell chemotaxis.

PDGF-D-induced facilitation of malignant mesothelioma cell migration was significantly inhibited by